A thalamo-amygdalar circuit underlying the extinction of remote fear memories

Bianca A. Silva[1], Simone Astori[2], Allison M. Burns[1], Hendrik Heiser[1,3], Lukas van den Heuvel[1,4], Giulia Santoni[1], Maria Fernanda Martinez-Reza[1], Carmen Sandi[2], Johannes Gräff[1*]

Affiliations

1 Laboratory of Neuroepigenetics, Brain Mind Institute, School of Life Sciences, École Polytechnique Fédérale Lausanne, CH-1015, Lausanne, Switzerland.

2 Laboratory of Behavioral Genetics, Brain Mind Institute, School of Life Sciences, École Polytechnique Fédérale Lausanne, CH-1015, Lausanne, Switzerland.

3 International Max Planck Research School "Neurosciences", Georg-August-Universität Göttingen, DE-37073 Göttingen, Germany.

4 Current address: Laboratory of Quantitative Neurosciences, Department of Bionanoscience, Delft University of Technology, 2629HZ Delft, The Netherlands.

*Correspondence to: johannes.graeff@epfl.ch

Abstract

Fear and trauma generate some of the longest-lived memories. Despite the corresponding need to better understand how enduring fear memories can be attenuated, the underlying brain circuits remain largely unknown. Here, using a combination of neuronal circuit mapping, *in vivo* fiber photometry, chemogenetic and closed-loop optogenetic manipulation of neuronal activity in mice, we show that the extinction of remote, i.e., 30-day old, fear memories depends on thalamic nucleus reuniens (NRe) inputs to the basolateral amygdala (BLA). We find that remote fear memory extinction activates NRe to BLA inputs, which are potentiated upon fear reduction. Furthermore, both monosynaptic NRe to BLA, and total NRe activity increase shortly before the end of freezing bouts during remote fear extinction, suggesting that the NRe registers and transmits extinction signals to the BLA. Accordingly, pan-NRe as well as pathway-specific NRe to BLA inhibition impairs, while their activation facilitates remote fear extinction. These findings provide the first functional description of the circuits underlying remote fear memory extinction and identify the NRe as a crucial upstream regulator of the BLA for this process.

Keywords

Fear extinction, remote memory, basolateral amygdala (BLA), nucleus reuniens (NRe) chemogenetics, DREADD, optogenetics, fiber photometry, contextual fear memory.

Introduction

Traumatic events generate some of the most enduring memories and can lead to chronic fear and stress-related conditions such as post-traumatic stress disorder (PTSD). The lifetime prevalence of PTSD in the general population is estimated at 7%[1,2], and this number at least quadruples among individuals having suffered severe traumata such as war or sexual assault[1,2]. One of the most effective measures against trauma-related disorders is a form of behavioral psychotherapy called exposure therapy[3,4]. This therapy consists of the repetitive exposure to reminders of the original traumatic memory in a safe environment, with the goal of progressively weakening the aberrant emotional responses associated with the fear-related memory[5]. Although exposure therapies are a reference intervention for PTSD[6], they lose efficacy the later they are applied after the original traumatic experience[7–10], which places strong emphasis on identifying treatment options for remote traumata[11,12].

Using fear extinction as an experimental model of exposure therapy, previous studies in both humans and animals have identified critical brain circuits that underlie fear memory attenuation[13–19]. However, the vast majority of these have focused on the neural correlates of extinction protocols applied shortly after the encoding of the traumatic memory (i.e., within the first day), leaving the role of extinction brain networks at remote timepoints poorly understood. This represents a gap of knowledge important to investigate as with age, traumatic memories undergo a systems consolidation process whereby the substrates of memory storage are re-organized[20–22]. Therefore, fear extinction for remote memories may not rely on the same canonical brain networks as for recent timepoints.

Results

Remote fear memory extinction activates an IL→NRe→BLA pathway, but not the monosynaptic IL→BLA pathway

Previous studies on recent (i.e., 1-2 day old) fear memory extinction in rodents have shown that the interplay between the medial prefrontal cortex (mPFC), in particular the infralimbic cortex (IL), and the basolateral amygdala (BLA) lies at the core of fear attenuation induced by exposure therapy-like extinction protocols[14,15,23,24]. However, the role of IL projections to the BLA (IL→BLA) has thus far not been investigated for remote fear memory extinction, although the BLA remains critically involved for recalling remote (i.e., 30-day old) fear memories[25–27] (Supplementary Fig. 1). To address this question, we combined retrograde tracing and cFos-based neuronal activity mapping to directly test the activation of IL→BLA neurons upon a previously established spaced fear extinction protocol that lastingly reduces both recent and remote traumatic memories[27,28] (Fig. 1a, b). Prior to the behavioral paradigm, we bilaterally injected the BLA with an *AAV2r-CAG::Tom* (Fig. 1a, c), which infects synaptic terminals and is retrogradely transported to pre-synaptic somata[29], and analyzed cFos expression in IL→BLA neurons after the last extinction session. We compared these data to control animals that did not receive shocks during the conditioning session (raw values of cFos counts and traced cells are given in Supplementary Fig. 2a-d). We found that in contrast to recent fear memory extinction, IL→BLA projecting neurons were not active following remote fear memory extinction (Fig. 1d, g).

To test for alternative pathways that may activate the BLA upon the extinction of remote fear memories[29], we screened for cFos induction in other brain areas identified by retrograde tracing (Supplementary Fig. 3a, b). We found that BLA-projecting neurons in the nucleus

reuniens of the thalamus (NRe, Fig. 1e; for precise definition of NRe boundaries see Methods section), and the ventral tegmental area (VTA, Supplementary Fig. 3c-f) were activated upon remote fear extinction. Since the NRe has previously been implicated as an important hub for the consolidation of remote memories[30–33], we reasoned that it may have a similar role for remote fear memory extinction and serve as a node between the IL and BLA. To test this hypothesis, we injected a retrogradely transported virus in the NRe (*AAV2r-CAG::GFP,* Fig. 1c) and assessed cFos activation in IL to NRe (IL→NRe) projections upon remote fear memory extinction. We found increased cFos activation in the IL→NRe neuronal population following remote fear memory extinction (Fig. 1f), which was largely non-overlapping with IL→BLA neurons (Supplementary Fig. 4), suggesting fear extinction induces activation of different IL outputs with memory age. Notably, AAV2-retrograde tracing results were confirmed by anterograde tracing (Supplementary Fig. 5) and by pseudotyped rabies-based tracing of inputs and outputs (TRIO)[34,35] (Supplementary Fig. 6). When we then analyzed IL→NRe and NRe→BLA activation upon recent fear memory extinction, we found no cFos increase in either of these projections (Fig. 1h, i, Supplementary Fig. 2e). Together, these results suggest that the circuits supporting fear extinction undergo a functional switch as memories age, and posit the NRe to be implicated in remote fear memory extinction.

Activity in the NRe bidirectionally modulates remote fear memory extinction

In order to test whether the NRe is directly participating in remote fear memory extinction, we then manipulated its activity during this process. To this end, we first inhibited NRe neurons by expressing the inhibitory designer receptor exclusively activated by designer drug (DREADD) hM4Di[34] via stereotaxic NRe injections of an *AVV8-hSyn::hM4Di-mCherry* (Fig. 2a) followed by daily clozapine-N-oxide (CNO, the DREADD agonist) administration at remote memory recall and during the extinction paradigm (Fig. 2b). We found that, as the extinction

protocol proceeded, CNO-treated animals retained significantly higher freezing levels as compared to vehicle-treated ones (Fig. 2b). This effect was also visible when the animals were tested for spontaneous recovery (SR) of the fear with a context re-exposure 14 days later, pointing to a persistent impairment of fear extinction upon NRe inactivation. Moreover, NRe inhibition during the extinction phase alone yielded a similar impairment of fear attenuation even upon CNO-free context exposure 14 days later (Supplementary Fig. 7a). In contrast, acute inhibition of the NRe only at SR did not affect freezing behavior (Supplementary Fig. 7b), suggesting that the NRe plays a crucial role in extinction learning, but not in extinction memory retrieval. Furthermore, CNO administration did not affect fear extinction in animals with off-target hM4Di-mCherry expression (i.e., with hM4Di expression outside the NRe, Supplementary Fig. 7c, d), which argues against unspecific CNO effects. Lastly, we observed no differences upon hM4Di-mediated NRe inhibition in overall locomotor activity in an open field test (Fig. 2c), indicating that the elevated freezing observed during the extinction paradigm was not due to an unspecific increase in immobility. Thus, a loss-of-function of NRe activity impairs remote fear memory extinction.

Next, we evaluated whether a gain-of-function of NRe activity might be beneficial for remote fear memory extinction. For this, we expressed the activatory DREADD hM3Dq[34] in excitatory NRe neurons by stereotaxic injections of *AAV8-CamKII::hM3Dq-mCherry* (Fig. 2d), which, upon systemic administration of CNO, induced activation in hM3Dq-mCherry transduced NRe neurons as revealed by cFos immunohistochemistry (Supplementary Fig. 8a, b). We found that CNO-mediated NRe activation during memory recall and each of the extinction sessions resulted in decreased freezing starting from the first context re-exposure (Fig. 2e). Importantly, chemogenetic NRe activation performed during extinction alone elicited a similar extinction facilitation (Supplementary Fig. 8c). Conversely, the same NRe activation protocol performed in the home cage, but in the absence of extinction training did not alter the animals' freezing

response upon context re-exposure one or fourteen days later (Supplementary Fig. 8d). Furthermore, chemogenetic NRe activation did not affect overall locomotor activity (Fig. 2f), excluding the possibility that changes in freezing responses were secondary to locomotor effects. These findings indicate that increasing NRe activity during extinction training facilitates fear memory attenuation.

NRe activity increases upon freezing cessation during remote fear memory extinction

To gain insight into the real-time activity of the NRe and its relation with the online freezing state of the animals during remote fear memory extinction, we next performed *in vivo* fiber photometry recordings in the NRe. To this end, we expressed the genetically encoded Ca^{2+} indicator GCaMP6f[35] in NRe excitatory neurons by local injection of *AAV1-CamKII::GCaMP6f*, and recorded Ca^{2+}-dependent and Ca^{2+}-independent fluorescence via an optical fiber implant at the injection site, through which we simultaneously delivered 465 nm and 405 nm excitation light[36] (Fig. 3a). Using a within-subject design, we compared NRe activity between context exposure before fear conditioning ("Habituation"), at memory recall thirty days post-conditioning ("Recall") and during each session of the spaced extinction protocol ("Extinction"), which expectedly reduced remote fear memories (Fig. 3b, c).

Upon temporal alignment of the photometry traces to freezing epochs, we observed a transient elevation in NRe activity starting shortly before the termination of freezing bouts during both recall and each of the extinction sessions (Fig. 3d, Supplementary Fig. 9a). Of note, this activation was not observed upon cessation of immobility bouts during habituation, showing it to be specifically related to fear responses (Fig. 3d). Furthermore, such dF/F transients were absent in the 405 nm traces, indicating that they were selectively related to Ca^{2+} signals and not to fiber motion artefacts. dF/F quantifications across subjects confirmed the significant

NRe activity increase upon freezing cessation during the recall and last extinction session but not during habituation (Fig. 3e, f). This increase in NRe activity was initiated approximately 500 ms prior to freezing termination, was most prominent around 200 ms before (Fig. 3g-i), and was not correlated with freezing initiation (Supplementary Fig. 9b, c). These findings show that the increase in NRe activity is time-locked to freezing cessation.

NRe activity mediates freezing cessation during remote memory extinction

In order to test whether such increase in NRe activity preceding freezing cessation could play a causal role in modulating freezing duration during remote fear memory extinction, we next manipulated the activity of NRe excitatory neurons time-locked to freezing behavior using a behavioral closed-loop optogenetic approach. For this, we coupled an online freezing detection system to a laser driver, so that photostimulation could be specifically triggered upon freezing (Fig. 4a). First, we used an optogenetic gain-of-function approach in animals expressing the activatory opsin Chronos[37] in NRe excitatory neurons (achieved by the combined NRe injection of *AAV1-CamKII::Cre* and *AAV1-FLEX-Chronos-GFP*, or its control *AAV1-FLEX-GFP*, Fig. 4b), which reliably induced action potentials at increasing stimulation frequencies (up to 20Hz) as revealed by *ex vivo* slice recordings (Supplementary Fig. 10a). When we applied the behavioral closed-loop photo-excitation of the NRe during remote fear memory extinction, we observed a shorter duration of freezing bouts (Fig. 4c), and an overall reduced latency to freezing cessation (Fig. 4d, e). These data indicate that an optogenetic stimulation of the NRe mimicking its naturally occurring increase upon freezing cessation facilitates fear attenuation.

To confirm these findings, we employed a behavioral closed-loop optogenetic inhibition approach by expressing the inhibitory opsin ArchT[38] in NRe excitatory neurons (achieved by

combined viral injections of *AAV1-CamKII::Cre* and *AAV1-FLEX-ArchT.GFP* into the NRe, or its control *AAV1-FLEX-GFP*) (Fig. 4f, g). When the NRe was photo-inhibited each time a freezing bout was detected during the remote fear memory extinction paradigm, we found an increased duration of freezing bouts (Fig. 4h), and an overall greater latency to freezing cessation (Fig. 4i, j). Together, these results indicate that NRe activity plays a crucial role in mediating the termination of freezing bouts during remote fear memory extinction.

NRe→BLA activity is time-locked to and mediates freezing cessation during remote fear memory extinction

In the following, we investigated how the NRe→BLA pathway, found to be activated upon remote fear memory extinction (Fig. 1e), might regulate this process. We first characterized the NRe→BLA connection in comparison to other known NRe outputs[39]. To this end, we injected animals with *AAV8-CamKII::hM3Dq-mCherry* in the NRe, and 90 min after CNO administration measured cFos expression in the mPFC, hippocampal area CA1, and the amygdala, which showed prominent mCherry$^+$ fiber density (Supplementary Fig. 11a). Of these, we found that only the BLA and lateral portion of the central amygdala (CeAl) were activated following chemogenetic NRe stimulation (Supplementary Fig. 11b, c).

Subsequently, we further characterized these amygdalar output regions of the NRe by optogenetic circuit mapping. We virally transduced the NRe with an *AAV1-hSyn::Chronos-Tom* (Supplementary Fig. 11d) and performed *ex vivo* whole-cell recordings in the CeA, and in principal neurons located in the BLA and the lateral amygdala (LA). Photostimulation of NRe fibers elicited excitatory postsynaptic currents (EPSCs) in all amygdalar sub-regions, but the responses were significantly (on average >10 times) larger in the BLA than in the CeA and LA (Supplementary Fig. 11e). EPSCs in BLA neurons also displayed lower paired-pulse ratio

than in the CeA and the LA, indicating higher release probability at NRe terminals innervating the BLA (Supplementary Fig. 11f). These results confirm NRe→BLA projectors as a major output connection of the NRe.

Next, we assessed the real-time engagement of this NRe→BLA pathway during remote fear memory extinction by pathway-specific *in vivo* fiber photometry. For this, we injected a retrogradely transported virus carrying Cre in the BLA (*AAV2r-pgk::Cre*), and a Cre-dependent GCaMP6f expressing virus (*AAV1-hSyn::FLEX-GCaMP6f*) in the NRe (Fig. 5a). We observed increased NRe→BLA activity prior to the end of freezing bouts during the recall and extinction sessions, but not prior to the end immobility bouts during habituation (Fig. 5b, c), in accordance with cFos mapping results at these timepoints (Supplementary Fig. 12). In line with the pan-NRe *in vivo* fiber photometry recordings (Fig. 3d, e), this finding suggests that during remote fear memory extinction, NRe→BLA projectors are specifically activated upon freezing cessation.

In order to test whether such increased activity in NRe→BLA neurons preceding freezing cessation can modulate freezing behavior during remote fear extinction, we then employed a pathway-specific behavioral closed-loop optogenetic stimulation protocol, analogous to the one used in Fig. 4a. For this, we injected a retrogradely transported virus carrying Cre in the BLA (*AAV2r-pgk::Cre*), a Cre-dependent Chronos expressing virus (*AAV1-hSyn::FLEX-Chronos-GFP* or its control *AAV1-hSyn::FLEX-GFP*) in the NRe, and stimulated NRe→BLA neurons time-locked to freezing behavior (Fig. 5d, e). Photostimulation of Chronos-expressing NRe terminals reliably induced postsynaptic currents at increasing stimulation frequencies (up to 20Hz) in the BLA, as revealed by *ex vivo* slice recordings (Supplementary Fig. 10b). We found that closed-loop optogenetic stimulation of NRe→BLA neurons during remote fear memory extinction led to a decreased duration of freezing bouts as compared to control

animals (Fig. 5e), and to an overall reduced latency to freezing cessation (Fig. 5f, g). This result indicates that NRe→BLA activity can directly induce termination of freezing bouts during remote fear memory extinction.

Synaptic plasticity in NRe→BLA output reflects remote fear memory extinction

The observation that activity in NRe→BLA projecting neurons is tightly related to freezing cessation throughout the remote fear extinction paradigm indicates that this pathway may be a major input to the BLA to encode remote fear extinction. To assess this, we first probed whether NRe→BLA connections undergo synaptic plasticity following efficient remote fear extinction by measuring the AMPA/NMDA EPSC ratio[40] in this pathway. We virally transduced the NRe with an *AAV1-hSyn::Chronos-Tom* and patched BLA neurons receiving inputs from the NRe *ex vivo* one day after the last extinction session (Fig. 5h, i). We found that remote fear memory extinction was accompanied by a significant increase in AMPA/NMDA ratio in the BLA, compared to remote fear recall alone and to control animals that either did not undergo the extinction or that did not receive foot shocks during conditioning but were exposed to the extinction procedure (Fig. 5j). Importantly, such increase in AMPA/NMDA ratio was not observed for recent fear memory extinction (Supplementary Fig. 13), in line with a lack of NRe→BLA activation at this timepoint (Fig. 1h). This finding shows that remote fear memory extinction specifically leads to synaptic potentiation of NRe→BLA inputs.

We then tested whether reduced synaptic potentiation in the NRe→BLA pathway might underlie fear extinction impairments. To this end, we measured the AMPA/NMDA ratio of NRe→BLA connections one day after the remote fear memory extinction paradigm performed under NRe chemogenetic inhibition, which prevented efficient fear memory extinction (Fig. 2b). In comparison to vehicle-treated animals showing efficient memory extinction, we found

blunted AMPA/NMDA ratio when the NRe activity was inhibited during extinction (Fig. 5k, lower panel). This finding suggests that an impairment of remote fear memory extinction is reflected by reduced synaptic plasticity in NRe→BLA outputs.

Next, we assessed whether artificially activating the NRe might induce such plasticity and ameliorate remote fear memory extinction. For this, we employed a suboptimal fear extinction protocol, in which animals received only a single context re-exposure (recall) 30 days after contextual fear conditioning, followed by no extinction training (i.e., the animals remained untested in their home cage on the subsequent days; Fig. 5l, upper panel). This protocol only partially reduced the animals' fear response as revealed by a test for their "extinction memory" the day after (VEH-treated animals in Fig. 5l). Correspondingly, this protocol did not induce plasticity in the NRe→BLA pathway (VEH-treated animals in Fig. 5m), which showed comparable AMPA/NMDA levels to control animals that did not undergo extinction (Fig. 5j). Conversely, when we repeatedly stimulated NRe activity by daily CNO administration even in the absence of extinction training, we observed increased AMPA/NMDA ratio in NRe→BLA projectors (CNO-treated animals in Fig. 5m). Importantly, such artificially induced potentiation was reflected by decreased freezing levels when the animals were tested for their "extinction memory" using the same behavioral paradigm (CNO-treated animals in Fig. 5l). This reduction of the freezing response was maintained even when the animals were re-exposed to the conditioned context 14 days later in the absence of CNO (Fig. 5l). Conversely, no fear reduction was observed when NRe activity was only stimulated once (Supplementary Fig. 14), or when repeated NRe stimulation was performed in the absence of context re-exposure (Supplementary Fig. 8d). These findings show that a repetitive artificial induction of NRe activity in combination with a suboptimal extinction paradigm leads to synaptic potentiation in NRe→BLA inputs and to a facilitation of remote fear memory extinction.

NRe→BLA projections are causally implicated in remote fear memory extinction

Lastly, we investigated whether the NRe→BLA pathway is causally implicated in regulating fear memory extinction by using a gain and loss-of-function approach (Fig. 6a, b). For the former, we expressed the excitatory DREADD hM3Dq (*AAV8-CamKII::hM3Dq-mCherry*) in the NRe, and activated NRe terminals in the BLA by repeated intra-amygdalar infusions of CNO in a suboptimal extinction paradigm identical to the one used for somatic NRe activation (Fig. 6c, upper panel). We found that mice receiving repeated CNO administration displayed improved fear extinction when re-exposed to the same context one day after the suboptimal extinction paradigm (Fig. 6c, lower panel), while their overall motor activity was not altered (Fig. 6d). Importantly, such freezing decrease was maintained upon context re-exposure in the absence of CNO 14 days later, indicating a persistent effect of NRe→BLA activation on extinction retention (Fig. 6c). Conversely, when we employed the same approach to stimulate NRe terminals in the hippocampus and the mPFC, two other NRe output areas (Supplementary Fig. 11a-c), which have previously been implicated in remote fear memory extinction[28,41], we observed no differences in freezing between CNO and vehicle-treated animals (Supplementary Fig. 15). These findings posit that the NRe conveys extinction-promoting signals via its inputs to the BLA, and that a gain-of-function of these projections facilitates fear memory extinction.

For the latter, we chemogenetically inhibited NRe→BLA projectors by *AAV8-hSyn::hM4Di-mCherry* injection into the NRe and micro-infusions of CNO into the BLA before each session of the regular remote fear extinction paradigm (Fig. 6e, upper panel). We found that the repeated inhibition of NRe→BLA neurons during the extinction paradigm impaired remote fear extinction (Fig. 6e, lower panel), without altering locomotor activity (Fig. 6f). Conversely, when we employed the same pathway-specific chemogenetic approach to inhibit another BLA input,

namely IL→BLA projectors, which did not show cFos activation upon remote fear memory extinction or recall (Fig. 1d, Supplementary Fig. 16a-c), we observed no differences in remote fear extinction efficacy (Supplementary Fig. 16d-e). Taken together, these results identify NRe→BLA afferents as a critical BLA input that mediates the extinction of remote fear memories.

Discussion

The present findings provide the first functional description of a neuronal circuit underlying remote fear memory extinction. Thereby, they address the paucity of research on this topic, which is surprising in light of the long-lasting nature of traumatic memories[42], the increased resistance of remote fear memories to disruption[43,44], and the decreased efficacy of exposure therapy with memory age[7–10].

Our findings stipulate that similar to memory consolidation, the brain circuits underlying fear extinction undergo a spatial shift over time. During consolidation, the neural substrates of fear memory storage have been found to re-organize, whereby memories become increasingly independent of anatomical structures subserving memory formation, such as the hippocampus, and progressively dependent on brain regions involved in long-term memory storage, such as cortical areas[20–22]. This indicates that the extinction of consolidated memories may similarly rely on a re-distributed network, likely requiring additional players to the canonical extinction-mediating pathways of recent memories. Indeed, during remote fear memory extinction we show that direct IL inputs to the BLA – a central pathway for recent fear extinction[14,15,23,24] – are not recruited (Fig. 1d, Supplementary Fig. 16d, e). Instead, we describe the engagement of an alternative input to the BLA for remote fear memory extinction, centered on the NRe.

We find that the NRe bidirectionally modulates remote fear extinction (Fig. 2) and that its activity is increased before the end of freezing epochs during remote fear memory extinction (Fig. 3). Moreover, by closed-loop optogenetic manipulations we show that NRe activity is sufficient to regulate freezing length during extinction (Fig. 4). Of note, the increased neuronal activity within the NRe occurs both during remote fear memory recall and its extinction (Fig.

3d-i, Supplementary Fig. 12), despite their opposite behavioral states. Since even a single memory recall session can trigger extinction[45,46], this finding suggests that the elevated NRe activity at remote recall may reflect a role in the initial stages of extinction-induced learning. Accordingly, chemogenetic NRe activation at remote recall shows an immediate extinction-facilitating effect (Fig. 2e), congruent with an incipient extinction process in the NRe, while chemogenetic inhibition has no effect on remote fear recall *per se*, but impairs fear attenuation during the later stages of the extinction paradigm (Fig. 2b). Consistent with such role of the NRe in extinction learning rather than memory storage are previous findings showing that NRe inhibition during remote memory recall does not affect remote memory retention[30,31,47]. These results are also reminiscent of prior evidence showing that NRe activity is required for changing mnemonic strategies in spatial memory tasks[48] and for preventing aberrant fear responses following a change in context[49]. Nevertheless, it remains to be determined whether within the NRe, extinction training leads to the formation of a new memory trace of safety referred to as "extinction learning"[15,17,19,46,50], or to an updating of the original memory trace of fear[51–55].

Downstream of the NRe, we find remote fear memory extinction to be mediated by excitatory monosynaptic projections from the NRe to the BLA (Fig. 1e, 5, 6). To our knowledge, this is the first description of an extra-amygdalar BLA input besides the well-established cortico-amygdalar projections[14,15,23,24] that regulates extinction. In particular, we find that the NRe→BLA pathway is active upon freezing cessation at both remote memory recall and at the end of the extinction procedure (Fig. 5b, c, Supplementary Fig. 12), while this connection shows an increased AMPA/NMDA ratio only after extinction training (Fig. 5i, j). This finding suggests that in the initial stages of extinction, the activity of NRe→BLA inputs is not sufficient to decrease freezing because of low synaptic strength, but gradually induces synaptic plasticity in this pathway as the extinction paradigm proceeds. Conversely, during late

extinction sessions, similar NRe→BLA activity levels (Fig. 5b, c) are likely to reduce freezing because the NRe→BLA synapse has undergone potentiation. In line with this interpretation, we find that preventing the NRe→BLA activation during remote fear memory extinction impairs fear attenuation (Fig. 2a, b) and is accompanied by blunted synaptic plasticity (Fig. 5k), while artificially increasing such plasticity leads to a concomitant facilitation of fear extinction (Fig. 5l, m). Since the BLA is part of an intra-amygdalar circuit implicated in extinction learning[15,56–61], such activation of NRe→BLA inputs may further trigger extinction-promoting amygdalar microcircuits[14], such as from the BLA to the CeAl[56] (Supplementary Fig. 11), but this remains to be experimentally determined. Moreover, it cannot be excluded that other BLA inputs, such as VTA→BLA projections[62–64] (Supplementary Fig. 3) may also contribute to remote fear extinction.

An additional functional NRe output for mediating remote fear extinction could be hippocampal area CA1, especially in light of its postulated role in retrieval suppression[65]. However, our data provide an initial indication against such scenario as chemogenetic activation of the NRe→CA1 pathway neither induces cFos activity in CA1 (Supplementary Fig. 11a-c), nor affects remote fear extinction efficiency (Supplementary Fig. 15c-d).

Upstream, the NRe is likely to receive contextual information from the IL, a brain area strongly implicated in extinction[15,66], whose projections to another midline thalamic nucleus, the paraventricular nucleus of the thalamus (PVT) have recently been related to extinction retrieval[67]. We find that IL→NRe projectors show cFos activation upon remote fear memory extinction (Fig. 1f, Supplementary Fig. 17a-c), and that optogenetic activation of this pathway facilitates fear attenuation during remote extinction (Supplementary Fig. 17d, e). These results are reminiscent of a previous report indicating that the inhibition of mPFC→NRe afferents impairs the extinction of recently acquired cued fear memories[68]. Nevertheless, here, by using

an unbiased neuronal mapping approach, we do not find IL→NRe afferents to be activated upon recent fear memory extinction (Fig. 1i; but this might depend on the exact extinction paradigm being used). Instead, we find IL→BLA projectors, which have previously been implicated in recent fear memory extinction[14,15,23,24], to be active (Fig. 1g, Supplementary Fig. 2e). Therefore, we hypothesize that although already relevant at recent timepoints, the IL→NRe projection becomes predominant for remote memories (Fig. 1f, Supplementary Fig. 2e, 17d, e), when the IL→BLA pathway is no longer active (Fig. 1d, Supplementary Fig. 16a-c) and, consequently, no longer functionally relevant to mediate extinction (Supplementary Fig. 16d, e). Such engagement of the IL→NRe at remote timepoints is also underscored by *in vivo* fiber photometry recordings (Supplementary Fig. 17f-h). Interestingly, although the activity of the IL→NRe pathway is enhanced at extinction, it is not time-locked to freezing cessation as the pan-NRe and NRe→BLA activities are (Fig. 3, 5a-c). Thus, the NRe is likely to integrate additional upstream information, the origins of which remain to be identified.

One possible type of information upstream to the NRe is that about internal state. Such information originates in lower order brain structures such as the hypothalamus[69], brainstem areas including the periaqueductal grey (PAG), or the VTA[70], from which the NRe receives dense inputs[71], and NRe stimulation has recently been shown to change the internal state of mice in response to perceived threats[72]. Accordingly, the increased NRe activity shortly before freezing cessation (Fig. 3) may reflect an internal state change, which is supported by the closed-loop optogenetic NRe manipulations that directly alter freezing behavior (Fig. 4).

Lastly, our findings contribute to paint a more general picture for the implication of midline thalamic nuclei in regulating fear memories at remote timepoints. So has the interplay between prefrontal cortical regions and midline thalamic nuclei[73] including the NRe[30,31,33,74] as well as the PVT[75] recently been found to be relevant for remote fear memory storage. Here, we identify

the NRe to route fear-related information from the IL to the BLA for remote fear memory extinction. Thus, in addition to the well-established direct cortico-amygdalar pathway underlying recent fear memory retrieval and extinction[14, 15, 23, 24], there appears to be an indirect cortico-thalamo-amygdalar route for fear processing that becomes dominant at remote times. When and how such spatiotemporal shift precisely occurs, remains to be investigated. Harnessing this knowledge will undoubtedly help to better understand how traumatic memories of different ages are being stored and can be attenuated.

Acknowledgments

We would like to thank Marion Curdy, Florian Wyler, Mattia Santoboni, Michael Kintscher, Forough Habibollahi, Romani Gros, Amelien Goossens, Célia Benquet, Denis Joly, Tania Hübscher, Ann-Riviere Warter, Lauriane Duvaud, Léa Ho Dac and Nana Sato for their contribution in histological procedures, the EPFL BIOP core facility for their technical assistance with image analysis, the Bertarelli Foundation Gene Therapy Core Facility at EPFL for AAV production and Luis de Lecea and Susan Tyree (Stanford) and Niccolò Banterle (EPFL) for their assistance with fiber photometry. **Funding**: BAS is supported by an EMBO long-term fellowship (ALT1605-2014, Marie Curie Actions, LTFCOFUND2013, GA-2013-609409. MFM-R was supported by an UNAM-DGECI International Scholarship from the National Autonomous University of Mexico. JG is a MQ fellow and a NARSAD Independent Investigator. HH is supported by a NENS Exchange Grant. The laboratory of JG is supported by the European Research Council (ERC-2015-StG 678832), by the Swiss National Science Foundation (SNSF), the National Competence Center for Research SYNAPSY (51NF40-185897) and by the Vallee Foundation. Work from CS laboratory was supported by the SNSF (31003A-176206 and SYNAPSY grants No. 158776 and 185897).

Author contributions

This study was planned and conceptualized by BAS and JG. BAS carried out the experiments and analyzed data. SA performed and analyzed electrophysiological experiments under the guidance of CS. AMB contributed to fiber photometry data analysis. GS contributed to viral injections and behavioral experiments. HH, LvdH and MFM-R contributed to histology and image analysis. The paper was written by BAS and JG and commented on by all authors.

Competing interests statement

The authors declare no competing interests.

Methods

Animals

Animals used were C57BL/6JRj male mice obtained from Janvier Labs, France. Animals were delivered at 5-7 weeks of age and allowed an acclimatization period of one week before testing. Animals between 8 and 13 weeks of age were used for behavioral experiments. All animals were housed at 22-25° C on a 12 h light-dark cycle (light on 7AM) with water and food *ad libitum*. Mice were housed in groups of 4 animals except for cFos analysis experiments where animals were single housed 2 days before sacrifice. All animals were handled according to protocols approved by the Swiss animal license VD2808 and VD2808.1.

NRe identification

Due to their homogeneity and small size, thalamic nuclei are often defined by vague anatomical criteria. Nonetheless, mouse brain atlases[76,77] indicate a division of the ventral portion of the midline thalamus (NRe) into several sub-nuclei including the nucleus reuniens (Re) medial xiphoid (Xi) and paraxiphoid (PaXi), the perireuniens nucleus (PR) or ventral reuniens nucleus (VRe), and the rhomboid nucleus (Rh). Due to their small size and close proximity, it is nearly impossible to distinguish the between the NRe sub-nuclei when performing local injections or lesions. Here, we refer to "NRe" as the combination of Re, Xi and PaXi as described elsewhere[76]. For cFos and retrograde studies, photometry and optogenetics NRe borders were very clearly defined, while, for chemogenetic manipulations some virus spillover in other ventral midline thalamic nuclei including the PR and Rh could not be avoided. cFos analysis, however, indicated that the Rh and PR are not recruited upon remote fear memory recall or extinction, nor are their projectors to the amygdala (data not

shown), suggesting that the virus spillover in these regions is unlikely to interfere with the observed results.

Behavioral testing

Contextual fear conditioning consisted of a 3 min habituation to the conditioning chamber (TSE Systems GmbH) followed by three 2 s foot shocks (0.8 mA) with an interval of 28 s. After the shocks, animals were kept in the conditioning chamber for an additional 15 s. One day (recent) or four weeks (remote) later, mice were re-exposed to the same chamber for 3 min without receiving the foot shock ("Recall") and returned to their home cage. On the following day, t underwent a spaced extinction protocol, for which they were re-exposed to the same context two times for three minutes each, separated by a 1 h intertrial interval, during which they were returned to their home cage. The same procedure was repeated for 4 days. Two weeks later, the spontaneous recovery (SR) of the extinguished memory was assessed by testing freezing during a 3 min exposure to the conditioning context. Animals belonging to the "No Shock" groups (Fig.1, 5, Supplementary Fig. 2, 3, 12, 13, 16, 17) underwent the same procedure but did not receive the foot shocks. For DREADD manipulation experiments, virus injection surgery was performed one week before (Fig.5k, Supplementary Fig. 7a, 15, 16) or one week after (Fig. 2, 5l, m, Supplementary Fig. 7b, d, 8c, d, 14) fear conditioning, and CNO (Sigma, 3 mg/kg) or vehicle was injected intraperitoneally 30 minutes before behavioral testing. For local CNO infusion experiments (Fig. 6, Supplementary Fig. 15, 16), virus injection surgery was performed 2 weeks before fear conditioning, and cannula implantation surgery was performed 5 weeks later. Ten minutes before behavioral testing, 150 nl of vehicle (0.9% NaCl, B. Braun) or CNO (150 µM) was injected bilaterally with an automatic pump (flow: 0.07 µl/min). For all DREADD/CNO experiments, CNO was dissolved in sterile 0.9% NaCl (B. Braun), which was administered as vehicle.

All behavioral testing was performed between 8AM and 12PM, and animals were randomly assigned to the different experimental groups. Percentage of time spent freezing over total context exposure time was automatically calculated with an infrared beam detection system (MultiConditioning System, TSE Systems GmbH). Freezing was quantified when absence of movement was detected for more than 0.5 s. Open field testing was performed in a circular arena where mice were left for 10 min to freely explore 30 min after vehicle of CNO IP-injections or 10 min after CNO micro-infusion into the BLA. Video tracking and quantification of locomotion in the open field were performed with the Ethovision tracking system.

Fiber photometry

Experiments were performed with a 1-site 2-color Fiber Photometry System (Doric Lenses, Canada) measuring both the 405 nm isosbestic and 465 nm calcium dependent GCaMP6f fluorescence on a single photodetector. Signals were recorded at 12 kHz using the built-in lock-in mode (Doric Neuroscience Studio). Briefly, 405 nm and 465 nm fiber-coupled-LEDs were sinusoidally modulated at 531 and 211 Hz, respectively, passed through an excitation filter and focused into a 400-µm fiber (NA 0.48) coupled to the mouse optic fiber implant. Emitted light was collected through the same fiber, passed through an emission filter and detected by a photoreceiver module (Newport 2151). The LED power was kept constant for every animal and every experimental session. Behavioral data from the TSE fear conditioning system were synchronized to the fluorescence data using a TTL pulse at the start and end of each session. Animals were habituated to the patch cord once a day for 5 days before the beginning of the behavioral experiment. At the start of each behavioral session, animals were connected to the patch cord in a neutral familiar housing cage, and baseline GCaMP6f signals were recorded for 3 minutes. Immediately thereafter, animals were gently transferred to the fear conditioning boxes for behavioral testing. Acquired data files were processed with custom-written codes in R (v.3.5.0)[78] and Igor Pro 8 (WaveMetrics). Photometry traces were

binned every 10 ms and aligned to freezing data generated by the TSE automatic infrared beam break-based scoring. Photometry traces were then low-pass filtered at 1.7 Hz using a Hanning filter (2.5 rejection band). 405 nm and 465 nm fluorescence signals were normalized within each session by calculating dF/F as (F-median(F_{bsl}))/median(F_{bsl}), where median(F_{bsl}) was calculated over the 3 min baseline. Before further data analysis, data were screened for recording stability using the 405 nm signal, and animals excluded from the analysis in case of loose fiber coupling, which resulted in large fluctuations in both signals.

To analyze traces at the end of freezing bouts, epochs of ± 2 s around the end of each freezing event were extracted (named hereafter $(dF/F)_{FrEnd}$), aligned and averaged within each behavioral session, regardless of the duration of the following mobility bout. Only freezing bouts longer than 1.5 s were used for this analysis. To assess changes of photometry signals at freezing end, $\Delta(dF/F)_{FrEnd}$ was calculated by subtracting mean values of $(dF/F)_{FrEnd}$ before (between -0.6 and -0.4 s) and after (between 0.0 and 0.2 s) freezing end (occurring at 0.0 s). The slope of the calcium dependent signal preceding freezing end was calculated as mean of the first derivative of $(dF/F)_{FreEnd}$ between -0.4 and 0.0 s. To calculate the time relative to the end of freezing of the steepest increase of $(dF/F)_{FreEnd}$, we calculated the time corresponding to the maximum of the first derivative of $(dF/F)_{FreEnd}$. The onset of the $(dF/F)_{FreEnd}$ rise was calculated as the time corresponding to the maximum of the third derivative of $(dF/F)_{FreEnd}$ around freezing end (from -0.8 to 0.2 s relative to freezing end). Signal power analysis (Supplementary Fig. 17h) was calculated as the sum of squares of the dF/F for each behavioral session $\Sigma(dF/F–average(dF/F))^2$.

Optogenetics experiments

Closed-loop optogenetic experiments: Two weeks after surgery mice were habituated for two days to the patch cord (200 µm diameter, 0.22 NA; Doric Lenses; 3 min each day). On the

following day, mice underwent CFC and recall 30 days later. No light was delivered during CFC and recall sessions although mice were connected to the patch cord. On the following day, during the first extinction session, mice with fiber optic implants were connected to the patch cord delivering blue light from a 473 nm laser (optogenetic activation) or yellow light from a 593 nm laser (optogenetic inhibition). Blue light was delivered for 2 s in 10-ms pulses at 20 Hz every time one freezing epoch exceeded 1s of duration, while yellow light was continuously delivered for 2s every time one freezing epoch exceeded 1s of duration. The light power at the fiber tip was about 10 mW. Real-time freezing behaviour was automatically detected with an infrared beam detection system (MultiConditioning System, TSE Systems GmbH). The photostimulation protocol was chosen based on previous results[62] showing that optogenetic stimulation of the NRe with these parameters has no unspecific effect on behaviour and that 20 Hz is within the physiological range of NRe neuronal firing.

IL→NRe optogenetic activation: Two weeks after animals received stereotactic viral injections and fiber implants, they underwent contextual fear conditioning. Thirty days later they received one recall session without light stimulation. On the following day animals underwent remote fear memory extinction with an intermittent light stimulation (20 Hz, 5s light ON, 5s light OFF, total duration=3min). Freezing time was calculated as the average time freezing across every light ON or light OFF epochs of the session.

Viral injections, NMDA injections, optic fiber and cannula implantation surgeries

For all surgical procedures mice were deeply anesthetized by subcutaneous injection of a mixture of fentanyl (0.05 mg/kg, Sintetica), midazolam (5 mg/kg, Actavis) and medetomidin (0.5 mg/kg, Orion Pharma). In addition, a solution containing lidocaine (6mg/kg) + bupivacaine (2.5 mg/kg) was injected subcutaneously at the site of incision. At the end of the surgical procedure an anesthesia reversal mix containing naloxone (1.2 mg/kg, Swissmedic), flumazenil (0.5 mg/kg, Actavis) and atipamezole (2.5 mg/kg, Orion Pharma) was injected

subcutaneously and animals were kept on a heating pad for an additional 2 h and were administered paracetamol (500 mg/250 mL/cage) in the drinking water for 5 days. All stereotaxic injections were performed using a glass pipette (intraMARK, 10-20 µm tip diameter, Blaubrand, injection flow: 0.1 *µ*l/min) connected to a syringe and a stereotaxic micromanipulator (Kopf Instruments). After injection the capillary was left at the injection site for 5 min before slow withdrawal to allow diffusion and minimize backflow.

For BLA bilateral lesions 300nl of NMDA (20 µg/µl, Sigma) dissolved in PBS were injected at -1.12 mm AP, ±3.28 mm ML and -4.95 mm DV (control animals were injected with the same volume of PBS).

For pan-NRe fiber photometry experiments, 300 nl of *AAV8-CamKII::GCaMP6f* ($2.3x10^{13}$, UPenn) were injected at a 15° off midline angle at -1.0 mm AP, -1.1 mm ML and -4.26 mm DV.

For NRe→BLA fiber photometry experiments, 2x300 nl of *AAV2r-Pgk::Cre* ($7.2x10^{12}$, Addgene) were injected bilaterally in the BLA at -1.12 mm AP, ±3.28 mm ML and -4.95 and 300 nl of *AAV1-hSyn::FLEX-GCaMP6f* ($1.9x10^{13}$, Addgene) were injected at a 15° off midline angle at -1.0 mm AP, -1.1 mm ML and -4.26 mm DV. For pan-NRe and NRe→BLA photometry experiments a 400 *µ*m fiber (Doric Lenses) was implanted 150 *µ*m above the NRe injection site. For IL→NRe fiber photometry experiments, 2x300 nl of *AAV2r-Pgk::Cre* ($7.2x10^{12}$, Addgene) were injected into the NRe at -0.85 mm A/P, 0 mm M/L, –4.2 mm D/V and -0.95 mm A/P, 0 mm M/L, –4.2 mm D/V and 300 nl of *AAV8-hSyn::FLEX-GCaMP6f* ($1.9x10^{13}$, Addgene) were injected in the IL at 1.94 mm AP, 0.5 mm ML and 2.8 mm DV and a 400 *µ*m fiber (Doric Lenses) was implanted 150 *µ*m above the IL injection site.

For pan-NRe optogenetic activation, 400 nl of a mix of *AAV1-CamKII::Cre* ($2.8x10^{13}$, Addgene) and *AAV1-Syn-FLEX-::Chronos-GFP* ($2.8x10^{12}$, UNC) or *AAV1-FLEX-CAG::GFP* (virus generously provided by Ralf Schneggenburger's lab) were injected into the NRe at -0.97 mm A/P, -1.1 mm M/L, –4.26 mm D/V. A 200 *µ*m fiber (0.39 NA, Thorlabs) was implanted 150 *µ*m

above the NRe injection site. The same coordinates were used for pan-NRe optogenetic inhibition experiments. The viral vectors used for optogenetic inhibition were: *AAV1-CamKII::Cre* ($2.8x10^{13}$, Addgene) and *AAV1-CAG-FLEX-::ArchT-GFP* ($4x10^{12}$, UNC) or *AAV1-FLEX-CAG::GFP* (virus generously provided by Ralf Schneggenburger's lab). For NRe→BLA optogenetic activation experiments, 2x300 nl of *AAV2r-Pgk::Cre* ($7.2x10^{12}$, Addgene) were injected bilaterally in the BLA and 300 nl *AAV1-Syn-FLEX-::Chronos-GFP* ($2.8x10^{12}$, UNC) or *AAV1-FLEX-CAG::GFP* were injected at a 15° off midline angle at -1.0 mm AP, -1.1 mm ML and -4.26 mm DV. A 200 μm fiber (0.39 NA, Thorlabs) was implanted 150 μm above the NRe injection site. For IL→NRe optogenetic activation experiments 2x300 nl of *AAV8-hSyn::Chronos-Tom* ($4.1x10^{13}$, Addgene) or a mix of *AAV1-CamKII::Cre* ($2.8x10^{13}$, Addgene) and *AAV8-hSynDIO::mCherry* ($2.3x10^{13}$, Addgene) were bilaterally injected in the IL at 2.00 mm AP, ±1.6 mm ML and -2.04 mm DV at a 30° off midline angle.

For DREADD experiments 2x300 nl of *AAV8-hSyn::hM4Di-mCherry* ($7.4x10^{12}$, UNC) or *AAV8-CamkII::hM3Dq-mCherry* ($9.7x10^{12}$, produced at the Bertarelli Foundation Gene Therapy Core Facility with a pAAV-CaMKIIa-hM3D(Gq)-mCherry gift from Bryan Roth, Addgene plasmid # 50476) were injected into the NRe at -0.85 mm A/P, 0 mm M/L, –4.2 mm D/V and -0.95 mm A/P, 0 mm M/L, –4.2 mm D/V. When controlling for CNO unspecific effects (Supplementary Fig. 7a) we injected *AAV8-hSyn::hM4Di-mCherry* ($7.4x10^{12}$, UNC) or a mix of *AAV1-CamKII::Cre* ($2.8x10^{13}$, Addgene) and *AAV8-hSynDIO::mCherry* ($2.3x10^{13}$, Addgene). The same coordinates were used to inject *AAV1-hSyn::Chronos-tdTom* ($4.1x10^{13}$, pAAV-Syn-Chronos-tdTomato was a gift from Edward Boyden, Addgene viral prep # 62726-AAV1) for patch clamp recordings.

For patch clamp recordings following chemogenetic manipulations of the NRe (Fig. 5k-m) the same virus was mixed with *AAV8-CamKII::hM4Di-mCherry* ($2.6x10^{13}$, Addgene) or *AAV8-CamkII::hM3Dq-mCherry* ($1.8x10^{12}$, VVF). For AAV2r retrograde tracing 2x300 nl of *AAV2r-CAG::Tom* ($7.2x10^{12}$, pAAV-CAG-tdTomato (codon diversified) was a gift from Edward

Boyden, Addgene viral prep # 59462-AAVrg) or *AAV2r-CAG::GFP* ($7x10^{12}$, pAAV-CAG-GFP was a gift from Edward Boyden, Addgene viral prep # 37825-AAVrg) were injected into the NRe at -0.85 mm A/P, 0 mm M/L, –4.2 mm D/V and -0.95 mm A/P, 0 mm M/L, –4.2 mm D/V and bilaterally into the BLA at -1.12 mm AP, ±3.28 mm ML and -4.95 mm DV.

For chemogenetic projection manipulations experiments, surgical implant of cannula guides into target sites was conducted 3 weeks after viral injections. For NRe→BLA terminals manipulation a 4 mm cannula guide (C315G/Spc) was implanted bilaterally at -1.5 mm AP, ±2.95 mm ML and -4.2 DV. For NRe→dCA1 a 1mm cannula guide was implanted at -2.0 mm AP, ±1.5 mm ML and -1.0 DV. For NRe→mPFC terminals stimulation experiments a 4 mm cannula guide was implanted bilaterally with at 30° off midline angle at 1.94 mm AP, - 1.85 mm ML and -1.2 mm DV. For IL→BLA terminals inhibition experiments 4x300 nl of *AAV8-CamKII::hM4Di-mCherry* ($2.6x10^{13}$, Addgene) was bilaterally injected in the IL at at 2.03 mm AP, ±1.6 mm ML and -2.44 mm DV and 2.13 mm AP, ±1.6 mm ML and -2.44 mm DV at a 30° off midline angle. A 4 mm cannula guide (C315G/Spc) was implanted bilaterally at -1.5 mm AP, ±2.95 mm ML and -4.2 DV. After one week of recovery, animals were habituated to non-protruding injectors once a day for three days. Local infusions of CNO and vehicle were performed with a 1 mm protruding injector 10 min before behavioral testing.

For TRIO experiments, 2x300 nl *of AAV2r-pgk::Cre* ($7.2x10^{12}$, Addgene) were injected bilaterally in the BLA and 2x400 nl of a mix of an *AAV1-CAG-FLEX-RabiesG-GFP* and *AAV1-CAG-FLEX-TVA* (produced at the Bertarelli Foundation Gene Therapy Core Facility) were injected into the NRe at -0.85 mm A/P, 0 mm M/L, –4.2 mm D/V and -0.95 mm A/P, 0 mm M/L, –4.2 mm D/V. Three weeks later 4x300 nl of an EnvA pseudotyped rabies virus in which the protein G was replaced by m-Cherry (*SADΔG-mCherry(EnvA)*; Salk Institute Vector Core) were injected into the NRe at -0.82 mm A/P, 0 mm M/L, –4.2 mm D/V; at -0.85 mm A/P, ±0.1 mm M/L, –4.2 mm D/V and -0.95 mm A/P, 0 mm M/L, –4.2 mm D/V and mice were sacrificed 8 days later. Control animals did not receive *AAV1-CAG-FLEX-RabiesG-GFP* injection.

Representative images of anatomical location for viral injections, optic fiber and cannula placements are shown with the corresponding experimental data or in Supplementary Fig. 18.

Electrophysiological recordings

Mice were deeply anaesthetized with isoflurane and decapitated. The brain was quickly removed, and 250-*μ*m thick coronal slices containing the amygdala were prepared using a vibrating tissue slicer (Campden Instruments,) in oxygenated (95% O_2 / 5% CO_2) ice-cold modified artificial CSF (ACSF), containing (in mM): 105 sucrose, 65 NaCl, 25 $NaHCO_3$, 2.5 KCl, 1.25 NaH_2PO_4, 7 $MgCl_2$, 0.5 $CaCl_2$, 25 glucose, 1.7 L(+)-ascorbic acid. After cutting, slices recovered for 1 h at 35°C in standard ACSF containing (in mM): 125 NaCl, 25 $NaHCO_3$, 2.5 KCl, 1.25 NaH_2PO_4, 1.2 $MgCl_2$, 2 $CaCl_2$, 18 glucose, 1.7 L(+)-ascorbic acid, and complemented with 2 sodium pyruvate and 3 myo-inositol. For current clamp recordings with somatic optogenetic stimulation, slices containing the ventromedial thalamus were superfused with oxygenated standard ACSF at nearly-physiological temperature (30-32°C). *AAV1-hSyn::Chronos-Tom* infected NRe cells were patched in the whole-cell configuration with borosilicate glass pipettes (TW150F-3, WPI) pulled with a DMZ-Zeitz puller (Zeitz-Instruments). Pipettes (3-4 MΩ) were filled with (in mM): 130 KGluconate, 10 KCl, 10 HEPES, 10 phosphocreatine, 0.2 EGTA, 4 Mg-ATP, 0.2 Na-GTP (290-300 mOsm, pH 7.2-7.3). NRe cell spiking was elicited by trains of 5-ms long whole-field LED flashes (470 nm CoolLED, 40 mW at objective exit) controlled via a Master-9 Pulse stimulator (A.M.P.Instruments). Reliability of photoactivation in eliciting cell spiking was tested using train stimulations at 5, 10 and 20 Hz. Spiking efficiency was calculated as percentage of LED flashes eliciting at least one action potential. For voltage clamp recordings with synaptic stimulation, slices containing the amygdala were superfused with ACSF at room temperature containing the $GABA_AR$ blocker picrotoxin (0.1 mM). Neurons identified with video-microscopy in the amygdala subnuclei were patched in the whole-cell configuration with borosilicate glass pipettes

(TW150F-3, WPI) pulled with a DMZ-Zeitz puller (Zeitz-Instruments). Pipettes (2-4 MΩ) were filled with (in mM): 120 CsGluconate, 10 CsCl, 10 HEPES, 10 phosphocreatine, 5 EGTA, 4 Mg-ATP, 0.2 Na-GTP, 2.5 QX-314-Cl^- (290-300 mOsm, pH 7.2-7.3). Visually identified neurons in the central amygdala (CeA), and pyramidal cells in the lateral (LA) and basolateral (BLA) amygdala displayed membrane capacitance values that were consistent with their cell size (CeA: 110 ± 14 pF, n = 11; LA: 173 ± 23 pF, n = 10; BA: 214 ± 6 pF, n = 67). BLA neurons that displayed a capacitance < 130 pF (on average 105 ± 9 pF, n = 20) were considered putative interneurons and excluded from the analysis. Thalamic afferents were photostimulated every 15 s with brief (1 ms) whole-field LED flashes (470 nm CoolLED) controlled via a Master-9 Pulse stimulator (A.M.P.Instruments).

For comparison of synaptic currents between different postsynaptic targets, the maximal LED power was applied (40 mW at objective exit). For paired-pulse ratio (PPR), AMPAR-mediated excitatory postsynaptic currents (AMPAR-EPSCs) were elicited at -70 mV by two consecutive photostimulations (50 ms interval), and the amplitude of the second response was divided by the amplitude of the first response. For AMPA/NMDA ratios, after recording AMPAR-EPSCs at -70 mV, the membrane potential was slowly switched to +40 mV, and DNQX (0.01 mM) was added to the perfusate to isolate the NMDA-EPSCs. In a subgroup of recordings, we verified that EPSCs elicited at +40 mV were blocked by the NMDAR antagonist D,L-APV (0.1 mM), which led to a current reduction of 95.8 ± 0.3% (n = 23). Peak values of AMPA-EPSCs were divided by the amplitude of NMDA-EPSCs, measured as the mean of 3 ms around the absolute peak. Series resistance (R_s) and input resistance (R_i) were monitored throughout recordings by brief voltage pulses, and data were rejected for changes in resistance >20%. Membrane voltage values were not corrected for liquid junction potential. Data were acquired through a Digidata1550A digitizer. Signals were amplified through a Multiclamp700B amplifier (Molecular Devices), sampled at 20 kHz and filtered at 10 kHz using Clampex10 (Molecular

Devices). Clampfit10 (Molecular Devices) and Igor Pro 6 (WaveMetrics) were used for data analysis.

Histology

For all histological analyses, mice were deeply anesthetized with pentobarbital (150 mg/kg intraperitoneally, Streuli Pharma) and perfused transcardially (4.0% paraformaldehyde, 1X PBS, pH 7.4). Brains were removed, post-fixed (4% PFA overnight), cryoprotected (30% sucrose, 1X PBS, 4° C, 48 h), frozen at -80°C and 40 μm coronal sections were cut with a sliding cryostat (Leica Microsystems). For cFos immunochemistry (IHC) mice were sacrificed 90 min after behavioral testing. For cFos IHC upon hM3Dq-mediated activation, CNO injection was performed 1 week after behavioral testing and animals were sacrificed 120 min after CNO or vehicle injection. Free floating sections were incubated in blocking solution (1% BSA, 1X PBS, 0.3% TritonX100, Sigma) at room temperature for 1 h, followed by incubation with rabbit anti-cFos antibody (1:5000, Synaptic System, #226 003) in blocking buffer (1% BSA, 1X PBS, 0.1% TritonX100) overnight at 4°C under constant shaking. Sections were washed extensively with PBS Triton 0.1% and then exposed to secondary antibody (Alexa Fluor 647-conjugated donkey anti-rabbit IgG, Life Technologies) in blocking buffer at room temperature for 2 h. They were incubated with Hoechst (Life Technologies) at 1:1000 in PBS at room temperature for 5 min, washed extensively with PBS and mounted on superfrost glass slides (ThermoScientific) with Fluoromount mounting medium (SouthernBiotech). Images were acquired on a virtual slide microscope (VS120, Olympus) with a 10X objective. For NeuN the same IHC procedure was used (rabbit Anti-NeuN antibody, 1:1000, Merk, #ABN78).

For verification of viral infection and cannulas/fiberoptic placement, one every two sections was stained with Hoechst, mounted and imaged with a VS120, 10X microscope.

Image analysis

For cFos, AAV2r, NeuN and Hoechst positive cell detection, images were analyzed with QuPath v0.1.3[79]. Briefly, brain areas were manually outlined based on the Hoechst signal following the Allen Brain Reference Atlas and positive cells within the outlined structures were automatically detected with the "positive cell detection" built-in function. The density of cFos positive cells ($cFos^+/mm^2$) was averaged over 2-6 sections per animal. For co-localization analysis of AAV2r, cFos and Hoechst positive cells a custom-built scrip for QuPath was used. Chance ratios were calculated for each outlined region with the following formulas and averaged across 2-6 sections for each animal: ($Double^+/Hoechst^+$)/chance level, where chance level was calculated as ($cFos^+/Hoechst^+$)x($AAV2r^+/Hoechst^+$). Chance ratios were then normalized by No shock controls (Fig. 1). Corresponding chance-normalized values before normalization to controls are reported in Supplementary Fig.12, Supplementary Fig.16, Supplementary Fig.17. Raw values of $cFos^+/Hoechst^+$ and $AAV2r^+/Hoechst^+$ are reported in Supplementary Fig. 2.

For anterograde tracing analysis (Supplementary Fig. 5), fiber density in the BLA and NRe was calculated as the mean mCherry or GFP intensity in the BLA or NRe normalized by background. Values were averaged across 2-6 sections per animal.

For verification of viral infection, the signal from the fluorescent reporter was manually thresholded and quantified (ImageJ). Infection efficiency (either % area or total area) was calculated over the total area of the nucleus as determined from the atlas overlay. Animals that showed less than 20% infection of the target area were excluded from the behavior analysis. Known anatomical target areas of the infected areas were carefully screened for possible off-site infection due to potential AAV transport. Optic fiber and cannula location were verified based on fiber tract lesion. AAV-Cre viruses location was verified in some cases by co-injection with fluorescently labeled cholera toxin B.

Statistical analysis

Data analysis was performed with PRISM 8 software (GraphPad). All data are reported as mean ± standard error. The target number of animals used in each experiment was determined based on numbers in previously published studies. The statistical test used, definition of *N*, and multiple hypothesis correction are described in the figure legends. For experiments in which animals were tested across multiple behavioral sessions repeated-measure statistical testing was applied. Statistical analyses details for each figure are reported in Supplementary Table 1.

References

1. Davidson, J. R. T., Stein, D. J., Shalev, A. Y. & Yehuda, R. Posttraumatic Stress Disorder: Acquisition, Recognition, Course, and Treatment. *J. Neuropsychiatry Clin. Neurosci.* **16**, 135-47 (2004).
2. Javidi, H. & Yadollahie, M. Post-traumatic Stress Disorder. *Int. J. Occup. Environ. Med.* **3**, 2–9 (2012).
3. Foa, E. B. & Kozak, M. J. Emotional processing of fear: exposure to corrective information. *Psychol. Bull.* **99**, 20–35 (1986).
4. Foa, E. B. Psychosocial treatment of posttraumatic stress disorder. in *Journal of Clinical Psychiatry* **67**, 40-5 (2006).
5. Cukor, J., Olden, M., Lee, F. & Difede, J. Evidence-based treatments for PTSD, new directions, and special challenges. *Ann. N. Y. Acad. Sci.* **1208**, 82–89 (2010).
6. Paintain, E. & Cassidy, S. First-line therapy for post-traumatic stress disorder: A systematic review of cognitive behavioural therapy and psychodynamic approaches. *Counselling and Psychotherapy Research* **18**, 237-50 (2018).
7. Costanzi, M., Cannas, S., Saraulli, D., Rossi-Arnaud, C. & Cestari, V. Extinction after retrieval: effects on the associative and nonassociative components of remote contextual fear memory. *Learn. Mem.* **18**, 508–518 (2011).

8. Gräff, J. *et al.* Epigenetic priming of memory updating during reconsolidation to attenuate remote fear memories. *Cell* **156**, 261–276 (2014).

9. An, X., Yang, P., Chen, S., Zhang, F. & Yu, D. An Additional Prior Retrieval Alters the Effects of a Retrieval-Extinction Procedure on Recent and Remote Fear Memory. *Front. Behav. Neurosci.* **11**, 259 (2018).

10. Kearns, M. C., Ressler, K. J., Zatzick, D. & Rothbaum, B. O. Early interventions for PTSD: A review. *Depression and Anxiety* **29**, 833–842 (2012).

11. McCleery, J. M. & Harvey, A. G. Integration of psychological and biological approaches to trauma memory: implications for pharmacological prevention of PTSD. *Journal of traumatic stress* **17**, 485-96 (2004).

12. Centonze, D., Siracusano, A., Calabresi, P. & Bernardi, G. Removing pathogenic memories: A neurobiology of psychotherapy. **32**, 123-32 *Mol. Neurobiol.* (2005).

13. Orsini, C. A. & Maren, S. Neural and cellular mechanisms of fear and extinction memory formation. *Neuroscience and Biobehavioral Reviews* **36**, 1773–1802 (2012).

14. Marek, R., Sun, Y. & Sah, P. Neural circuits for a top-down control of fear and extinction. *Psychopharmacology* **236**, 313-20 (2019).

15. Herry, C. *et al.* Neuronal circuits of fear extinction. *European Journal of Neuroscience* **31**, 599–612 (2010).

16. Fullana, M. A. *et al.* Fear extinction in the human brain: A meta-analysis of fMRI studies in healthy participants. *Neuroscience and Biobehavioral Reviews* **88**, 16-25 (2018).

17. Pape, H.-C. & Pare, D. Plastic Synaptic Networks of the Amygdala for the Acquisition, Expression, and Extinction of Conditioned Fear. *Physiol. Rev.* **90**, 419-36 (2010).

18. Milad, M. R. & Quirk, G. J. Fear Extinction as a Model for Translational Neuroscience: Ten Years of Progress. *Annu. Rev. Psychol.* **63**, 129-51(2012).

19. Myers, K. M. & Davis, M. Mechanisms of fear extinction. *Molecular Psychiatry* **12**, 120–150 (2007).

20. Frankland, P. W. & Bontempi, B. The organization of recent and remote memories. *Nat. Rev. Neurosci.* **6**, 119–30 (2005).

21. Albo, Z. & Gräff, J. The mysteries of remote memory. *Philosophical Transactions of the Royal Society B: Biological Sciences* **373**, 1742 (2018).

22. Tonegawa, S., Morrissey, M. D. & Kitamura, T. The role of engram cells in the systems consolidation of memory. *Nature Reviews Neuroscience* **19**, 485-98 (2018).

23. Knapska, E. *et al.* Functional anatomy of neural circuits regulating fear and extinction. *Proc. Natl. Acad. Sci. U. S. A.* **109**, 17093-8 (2012).

24. Bloodgood, D. W., Sugam, J. A., Holmes, A. & Kash, T. L. Fear extinction requires infralimbic cortex projections to the basolateral amygdala. *Transl. Psychiatry* **8**, 60 (2018).

25. Gale, G. D. *et al*. Role of the basolateral amygdala in the storage of fear memories across the adult lifetime of rats. *Journal of Neuroscience,* **24**, 3810-3815 (2014).

26. Kitamura, T. *et al.* Engrams and circuits crucial for systems consolidation of a memory. *Science (80-.).* **356**, 73–78 (2017).

27. Silva, B. A., Burns, A. M. & Gräff, J. A cFos activation map of remote fear memory attenuation. *Psychopharmacology* **236**, 369-81 (2019).

28. Khalaf, O. *et al.* Reactivation of recall-induced neurons contributes to remote fear memory attenuation. *Science* **360**, 1239-42 (2018).

29. Tervo, D. G. R. *et al.* A Designer AAV Variant Permits Efficient Retrograde Access to Projection Neurons. *Neuron* **92**, 372-82 (2016).

30. Vetere, G. *et al.* Chemogenetic Interrogation of a Brain-wide Fear Memory Network in Mice. *Neuron* **94**, 363-74 (2017).

31. Sierra, R. O. *et al.* Reconsolidation-induced rescue of a remote fear memory blocked by an early cortical inhibition: Involvement of the anterior cingulate cortex and the mediation by the thalamic nucleus reuniens. *Hippocampus* **27**, 596-607 (2017).

32. Troyner, F., Bicca, M. A. & Bertoglio, L. J. Nucleus reuniens of the thalamus controls fear memory intensity, specificity and long-term maintenance during consolidation. *Hippocampus* **28**, 602-16 (2018).

33. Hallock, H. L., Wang, A. & Griffin, A. L. Ventral Midline Thalamus Is Critical for Hippocampal-Prefrontal Synchrony and Spatial Working Memory. *J. Neurosci.* **155**, 78-85 (2016).

34. Armbruster, B. N., Li, X., Pausch, M. H., Herlitze, S. & Roth, B. L. Evolving the lock to fit the key to create a family of G protein-coupled receptors potently activated by an inert ligand. *Proc. Natl. Acad. Sci. U. S. A.* **104**, 5163–5168 (2007).

35. Chen, T. W. *et al.* Ultrasensitive fluorescent proteins for imaging neuronal activity. *Nature* **499**, 295-300 (2013).

36. Barnett, L. M., Hughes, T. E. & Drobizhev, M. Deciphering the molecular mechanism responsible for GCaMP6m's Ca2+-dependent change in fluorescence. *PLoS One* **12**, e0170934 (2017).

37. Klapoetke, N. C. *et al.* Independent optical excitation of distinct neural populations. *Nat. Methods* **11**, 338-46 (2014).

38. Han, X. *et al.* A high-light sensitivity optical neural silencer: development and application to optogenetic control of non-human primate cortex. *Frontiers in systems neuroscience* **5**, 18 (2011).

39. Vertes, R. P. *et al.* Efferent projections of reuniens and rhomboid nuclei of the thalamus in the rat. *Journal of comparative neurology* **499**, 768-796 (2006)

40. Kim, W. Bin & Cho, J. H. Encoding of Discriminative Fear Memory by Input-Specific LTP in the Amygdala. *Neuron* **95**, 1129-46 (2017).

41. Vetere, G., Restivo, L. & Ammassari-Teule, M. Pre-synaptic control of remote fear extinction in the neocortex. *Front. Behav. Neurosci.* **6**, (2012).

42. APA. *American Psychiatric Association, 2013. Diagnostic and statistical manual of*

mental disorders (5th ed.). *American Journal of Psychiatry* (2013).

43. Milekic, M. H. & Alberini, C. M. Temporally graded requirement for protein synthesis following memory reactivation. *Neuron* **36**, 521–525 (2002).

44. Frankland, P. W. *et al.* Stability of recent and remote contextual fear memory. *Learn. Mem.* **13**, 451-7 (2006).

45. Baldi, E., & Bucherelli, C. Brain sites involved in fear memory reconsolidation and extinction of rodents. *Neuroscience & Biobehavioral Reviews* **53**, 160-190 (2015).

46. Bouton, M. E. Context and Behavioral Processes in Extinction. *Learn. Mem.* **11**, 485–494 (2004).

47. Loureiro, M. *et al.* The Ventral Midline Thalamus (Reuniens and Rhomboid Nuclei) Contributes to the Persistence of Spatial Memory in Rats. *J. Neurosci.* **32**, 9947–9959 (2012).

48. Cholvin, T. *et al.* The Ventral Midline Thalamus Contributes to Strategy Shifting in a Memory Task Requiring Both Prefrontal Cortical and Hippocampal Functions. *J. Neurosci.* **33**, 8772-83 (2013).

49. Xu, W. & Südhof, T. C. A Neural CIrcuit for Memory Specificty and Generalization. *Science (80-.).* **339**, 1290–1295 (2013).

50. Quirk, G. J. & Mueller, D. Neural mechanisms of extinction learning and retrieval. *Neuropsychopharmacology* **33**, 56-72 (2008).

51. Tronson, N. C. & Taylor, J. R. Molecular mechanisms of memory reconsolidation. *Nat. Rev. Neurosci.* **8**, 262–75 (2007).

52. Monfils, M. H., Cowansage, K. K., Klann, E. & Ledoux, J. E. Extinction-Reconsolidation boundaries: Key to persistent attenuation of fear memories. *Science (80-.).* **324**, 951–955 (2009).

53. Clem, R. L. & Schiller, D. New Learning and Unlearning: Strangers or Accomplices in Threat Memory Attenuation? *Trends in Neurosciences* **39**, 340-51 (2016).

54. Nader, K. & Hardt, O. A single standard for memory: The case for reconsolidation. *Nature Reviews Neuroscience* **10**, 224-34 (2009).

55. Troyner, F. & Bertoglio, L. J. Nucleus reuniens of the thalamus controls fear memory reconsolidation. *Neurobiol. Learn. Mem.* **177**:107343 (2021).

56. Ehrlich, I. *et al.* Amygdala Inhibitory Circuits and the Control of Fear Memory. *Neuron* **62**, 757–771 (2009).

57. Song, Z., Chen, H., Xu, W., Wu, S. & Zhu, G. Basolateral amygdala calpain is required for extinction of contextual fear-memory. *Neurobiol. Learn. Mem.* **155**, 180-88 (2018).

58. Herry, C., Trifilieff, P., Micheau, J., Lüthi, A. & Mons, N. Extinction of auditory fear conditioning requires MAPK/ERK activation in the basolateral amygdala. *Eur. J. Neurosci.* **24**, 261-9 (2006).

59. Falls, W. A., Miserendino, M. J. D. & Davis, M. Extinction of fear-potentiated startle: Blockade by infusion of an NMDA antagonist into the amygdala. *J. Neurosci.* **12**, 854-63 (1992).

60. Mao, S. C., Hsiao, Y. H. & Gean, P. W. Extinction training in conjunction with a partial agonist of the glycine site on the NMDA receptor erases memory trace. *J. Neurosci.* **26**, 8892-9 (2006).

61. Lu, K. T., Walker, D. L. & Davis, M. Mitogen-activated protein kinase cascade in the basolateral nucleus of amygdala is involved in extinction of fear-potentiated startle. *J. Neurosci.* **21**, 162 (2001).

62. Johansen, J. P., Tarpley, J. W., LeDoux, J. E. & Blair, H. T. Neural substrates for expectation-modulated fear learning in the amygdala and periaqueductal gray. *Nat. Neurosci.* **13**, 979–86 (2010).

63. Likhtik, E., Popa, D., Apergis-Schoute, J., Fidacaro, G. a & Paré, D. Amygdala intercalated neurons are required for expression of fear extinction. *Nature* **454**, 642–645 (2008).

64. Salinas-Hernández, X. I. *et al.* Dopamine neurons drive fear extinction learning by signaling the omission of expected aversive outcomes. *Elife* **7**, e38818 (2018).

65. Anderson, M. C., Bunce, J. G. & Barbas, H. Prefrontal–hippocampal pathways underlying inhibitory control over memory. *Neurobiology of Learning and Memory.* **134**, 145-161 (2016).

66. Rosas-Vidal, L. E., Do-Monte, F. H., Sotres-Bayon, F. & Quirk, G. J. Hippocampal-prefrontal BDNF and memory for fear extinction. *Neuropsychopharmacology* **39**, 2161–2169 (2014).

67. Tao, Y. *et al.* Projections from Infralimbic Cortex to Paraventricular Thalamus Mediate Fear Extinction Retrieval. *Neurosci. Bull.* (2020).

68. Ramanathan, K. R., Jin, J., Giustino, T. F., Payne, M. R. & Maren, S. Prefrontal projections to the thalamic nucleus reuniens mediate fear extinction. *Nat. Commun.* **9**, 4527 (2018).

69. Silva, B. A., Gross, C. T. & Gräff, J. The neural circuits of innate fear: detection, integration, action, and memorization. *Learn. Mem.* **23**, 544–555 (2016).

70. Lammel, S., Lim, B. K. & Malenka, R. C. Reward and aversion in a heterogeneous midbrain dopamine system. *Neuropharmacology* **76**, 351-9 (2014).

71. McKenna, J. T. & Vertes, R. P. Afferent projections to nucleus reuniens of the thalamus. *J. Comp. Neurol.* **480**, 115–142 (2004).

72. Salay, L. D., Ishiko, N. & Huberman, A. D. A midline thalamic circuit determines reactions to visual threat. *Nature* **557**, 183-89 (2018).

73. DeNardo, L. A. *et al.* Temporal evolution of cortical ensembles promoting remote memory retrieval. *Nat. Neurosci.* **22**, 460-469 (2019).

74. Wheeler, A. L. *et al.* Identification of a Functional Connectome for Long-Term Fear Memory in Mice. *PLoS Comput. Biol.* **9**, (2013).

75. Do-Monte, F. H., Quinõnes-Laracuente, K. & Quirk, G. J. A temporal shift in the circuits mediating retrieval of fear memory. *Nature* **519**, 460–463 (2015).

76. Paxinos, G. & Franklin, K. B. J. The mouse brain in stereotaxic coordinates. *Acad. Press* 1–350 (2001).

77. Sunkin, S. M. *et al.* Allen Brain Atlas: An integrated spatio-temporal portal for exploring the central nervous system. *Nucleic Acids Res.* **41**, 996-1008 (2013).

78. R Core Team. R: A language and environment for statistical computing. http://www.R-project.org/. *R Foundation for Statistical Computing, Vienna, Austria* (2017).

79. Bankhead, P. *et al.* QuPath: Open source software for digital pathology image analysis. *Sci. Rep.* **7**, 16878 (2017).

Fig. 1. Recent fear memory extinction activates IL to BLA inputs, whereas remote fear extinction recruits an IL→NRe→BLA pathway. (a) Schematic representation of the behavioral paradigm for remote (top) and recent (bottom) fear memory extinction. Fifteen days after viral tracer injection mice underwent contextual fear conditioning (CFC). Thirty days (remote, top) or one day (recent, bottom) later, animals were re-exposed to the conditioned context in the absence of foot shock (Recall) and, subsequently, to the spaced remote fear memory extinction paradigm consisting of two sessions of context exposure per day for four days. Control animals did not receive foot shocks during fear conditioning, but underwent the extinction procedure (No shock). **(b)** Freezing levels during recall and the last extinction session (Extinction) of the remote (left) and recent (right) fear memory extinction paradigm compared to freezing levels in control animals. Remote: One-way ANOVA, $F(2, 21)=7.13$, $P=0.004$, multiple comparison, Holm-Sidak, * $P<0.05$, ** $P<0.01$; Recent: One-way ANOVA, $F(2, 15)=5.32$, $P=0.018$, multiple comparison, Holm-Sidak, * $P<0.05$, ** $P<0.01$. N=6-10 animals/ behavioural group. **(c)** Schematic representation (top) and example pictures (bottom) of the retrograde virus injection strategy. Scale bar: 1mm **(d)** Representative picture (left) and colocalization analysis (right) of retrogradely traced cells from the BLA ($AAV2r^+$) and cells activated in the IL ($cFos^+$) in the remote extinction and the no shock control group. Unpaired t-test, $P=0.748$, N=8-9 animals/behavioral group. **(e)** Example picture (left) and colocalization analysis (right) of retrogradely traced cells from the BLA ($AAV2r^+$) and cells activated in the NRe ($cFos^+$) in the remote extinction and the no shock control group. Unpaired t-test, $P=0.024$, N=6-11 animals/behavioral group. **(f)** Example picture (left) and colocalization analysis (right) of retrogradely traced cells from the NRe ($AAV2r^+$) and cells activated in the IL ($cFos^+$) in the remote extinction and the no shock control group. Unpaired t-test, $P=0.0003$, N=7-9 animals/behavioral group. **(g)** Representative picture (left) and colocalization analysis (right) of retrogradely traced cells from the BLA ($AAV2r^+$) and cells activated in the IL ($cFos^+$) in the recent extinction and the no shock control group. Unpaired t-test, $P=0.0459$, N=7-8

animals/behavioral group. **(h)** Example picture (left) and colocalization analysis (right) of retrogradely traced cells from the BLA ($AAV2r^+$) and cells activated in the NRe ($cFos^+$) in the recent extinction and the no shock control group. Unpaired t-test, P=0.31, N=8-10 animals/behavioral group. **(i)** Example picture (left) and colocalization analysis (right) of retrogradely traced cells from the NRe ($AAV2r^+$) and cells activated in the IL ($cFos^+$) in the recent extinction and the no shock control group. Unpaired t-test, P=0.57, N=10 animals/behavioral group; scale bar = 100μm. Arrowheads indicate double positive cells ($AAV2r^+$, $cFos^+$). BLA, basolateral amygdala; CFC, contextual fear conditioning; Ext, extinction; IL, infralimbic cortex; NRe, nucleus reuniens of the thalamus. Data are represented as mean ±SEM. Statistical analysis details for each figure panel are reported in Supplementary Table 1.

Fig. 2. The NRe bidirectionally modulates remote fear memory extinction. (a) (Top) Schematic representation of *AAV8-hM4Di-mCherry* injection in the NRe. (Bottom) Representative picture of hM4Di-mCherry expression in the NRe scale bar = 500μm. **(b)** (Top) Experimental timeline. All animals underwent contextual fear conditioning (CFC) and were injected with *AAV8-hSyn::hM4Di-mCherry* one week later. Thirty days after CFC, the animals underwent memory recall, the spaced extinction procedure and a test for spontaneous recovery of the fear (SR) under CNO or vehicle treatment (VEH). (Bottom) Freezing responses during the remote fear memory extinction paradigm and SR upon hM4Di/CNO-mediated inhibition of the NRe or its vehicle control. Yellow bars indicate days of CNO or VEH administration. Two-way RM ANOVA, VEH vs CNO: $F(1, 45)=5.696$, $P=0.02$, multiple comparison, Sidak, ** $P<0.01$, N=10-37 animals/group. **(c)** Locomotion analysis in an open field arena upon hM4Di/CNO-mediated inhibition of the NRe. Unpaired t-test, $P=0.53$. N=7-8 animals/group. **(d)** (Top) Schematic representation of *AAV8-hM3Dq-mCherry* injection in the NRe. (Bottom) Representative picture of hM3Dq-mCherry expression in the NRe scale bar = 500μm. **(e)** (Top) Experimental timeline. All animals underwent CFC and were injected with *AAV8-CamKII::hM3Dq-mCherry* one week later. Thirty days after CFC, the animals underwent memory recall, the spaced extinction procedure and a SR test under CNO or vehicle treatment. (Bottom) Freezing responses during the remote fear memory extinction paradigm and SR upon hM3Dq-mediated activation of the NRe. Blue bars indicate CNO or VEH exposure. Two-way RM ANOVA, VEH vs CNO: $F(1, 9)=14.01$, $P=0.0046$, multiple comparison, Sidak, * $P<0.05$, ** $P<0.01$, *** $P< 0.001$, N=5-6 animals/ behavioral group. **(f)** Locomotion analysis in an open field arena upon hM3Dq-mediated activation of the NRe. Unpaired t-test, $P=0.64$, N=14-15 animals/group. BL, baseline freezing upon novel context exposure; CFC, contextual fear conditioning; CNO, clozapine-N-oxide; NRe, nucleus reuniens of the thalamus; Rec, recall; SR, spontaneous recovery; VEH, vehicle. Data are represented

as mean ±SEM. Statistical analysis details for each figure panel are reported in Supplementary Table 1.

Fig. 3. Freezing cessation during remote fear memory recall and extinction is accompanied by increased NRe activity. (a) Schematic representation of the fiber photometry recording implant (left) and representative picture of GCaMP6f expression and localization of the optical fiber implant in the NRe (right). Scale bar = 200μm. **(b)** Schematic representation of the experimental setup. Forty days after fiber optic implantation, animals were exposed to the conditioned context in the absence of shock once a day for 3 days and connected to the patch cord for Habituation (Hab). On the following day, mice underwent contextual fear conditioning (CFC). Animals were re-exposed to the conditioned context 30 days later in the absence of foot shock (Recall) and, subsequently, to the spaced extinction paradigm consisting of two sessions of context exposure per day for four days. Fifteen days later animals received an additional context exposure to test for the spontaneous recovery of the fear response (SR). Five minutes before each behavioral session, animals were connected to the patch cord, and photometry recording was started. **(c)** Freezing levels during Habituation, Recall, the last extinction session (Ext) and SR. One-way RM ANOVA for Rec, Ext and SR, $F(2, 8)=31.1$, $P=0.0002$, multiple comparison, Sidak, *** $P<0.001$. N=5 animals. **(d)** (Left) Example traces of photometry signals (reported as dF/F, see Methods) generated by 465 nm (black, Ca^{2+}-dependent) and 405 nm (blue, Ca^{2+}-independent) LED excitation during habituation, recall and the last extinction session. Blue boxes above the traces indicate freezing bouts (0.5s ≥ light blue < 1.5s; dark blue ≥1.5s). (Boxed) Expanded portions of the traces on the left, relating NRe activity and freezing bouts. (Right) Mean dF/F signal ±2s around freezing cessation (indicated by the dashed line, 0s) for ≥1.5s freezing bouts from the corresponding behavioral session in the left panel. **(e)** Quantification of dF/F difference before and after freezing end. One-way ANOVA, $F(2, 11)=16.96$, $P=0.0004$, multiple comparison, Sidak, ** $P<0.01$, *** $P<0.001$, N=4-5 animals/timepoint. Two-tailed one-sample t-test (theoretical mean=0), # $P<0.01$, N=4-5 animals/timepoint. **(f)** Quantification of dF/F mean slope during the 0.4s interval before freezing end. One-way ANOVA, $F(2, 11)=20.25$,

P=0.0002, multiple comparison, Sidak, ** P<0.01, *** P<0.001, N=4-5 animals/timepoint. Two-tailed one-sample t-test (theoretical mean=0), # P<0.01, N=4-5 animals/timepoint. **(g)** Illustration of the first and third derivative of mean dF/F around freezing end used to calculate the signal onset (ON) and latency of steepest rise (S) relative to freezing cessation (dashed line, 0s). **(h)** Quantification of signal onset latency relative to freezing end. Two-tailed one-sample t-test (theoretical mean=0), # P<0.01, N=5 animals/timepoint. **(i)** Quantification of steepest rise latency relative to freezing end. Two-tailed one-sample t-test (theoretical mean=0), # P<0.05, N=5 animals/timepoint. CFC, contextual fear conditioning; Ext, extinction; Hab, habituation; NRe, nucleus reuniens of the thalamus; Rec, recall; SR, spontaneous recovery. Data are represented as mean ±SEM. Statistical analysis details for each figure panel are reported in Supplementary Table 1.

Fig. 4. Behavioral closed-loop optogenetic manipulation of the NRe during remote fear memory extinction bidirectionally modulates freezing cessation. (a) Schematic representation of the behavioral closed-loop optogenetic activation experimental strategy: Real-time freezing detection triggers NRe photostimulation (20 Hz, 2 s) after each freezing bout of ≥ 1s. **(b)** (Left) Schematic representation of the optogenetic fiber optic implant; (right) representative picture of Chronos-GFP expression in NRe excitatory neurons achieved by co-infection of an *AAV1-CamKII::Cre* and *AAV1-Syn::FLEX-Chronos-GFP*, and localization of the optical fiber implant in the NRe. Scale bar = 100μm. **(c)** Example of freezing cessation upon NRe photostimulation (blue shading) in an *AAV1-GFP* (left) and *AAV1-Chronos-GFP* (right) injected animal. Freezing bouts are ordered by freezing epoch duration. **(d)** Latency to freezing cessation upon NRe behavioral closed-loop optogenetic stimulation in *AAV1-GFP* and *AAV1-Chronos-GFP* injected animals. Two-tailed t-test (Welch-corrected), P=0.03, N=4-5 animals/group. **(e)** Distribution analysis of latency to freezing cessation from light stimulation onset in *AAV1-GFP* and *AAV1-Chronos-GFP* injected animals (bin width: 300 ms); Kolmogorov-Smirnov test, P=0.0007, N=221-242 latencies/behavioral group, 4-5 animals/group. **(f)** Schematic representation of the behavioral closed-loop optogenetic inhibition experimental strategy. Real-time freezing detection triggers NRe photoinhibition (continuous, 2 s) after each freezing bout of ≥ 1s. **(g)** (Left) Schematic representation of the optogenetic fiber optic implant; (right) representative picture of ArchT-GFP expression in NRe excitatory neurons achieved by co-infection of an *AAV1-CamKII::Cre* and *AAV1-Syn::FLEX--ArchT-GFP*, and localization of the optical fiber implant in the NRe. Scale bar = 100μm. **(h)** Example of freezing cessation upon NRe photoinhibition (orange shading) in an *AAV1-GFP* (Left) and *AAV1-ArchT-GFP* (Right) injected animal. Freezing bouts are ordered by freezing epoch duration. **(i)** Latency to freezing cessation upon NRe behavioral closed-loop optogenetic inhibition in *AAV1-GFP* and *AAV1-ArchT-GFP* injected animals. Two-tailed t-test (Welch-corrected), P=0.017, N=6 animals/group. **(j)** Distribution analysis of latency to freezing

cessation from light stimulation onset in *AAV1-GFP* and *AAV1-ArchT-GFP* injected animals (bin width: 300 ms); Kolmogorov-Smirnov test, $P<0.0001$, N=148-170 latencies/behavioral group, 6 animals/group. Data in bar charts are represented as mean ±SEM. Statistical analysis details for each figure panel are reported in Supplementary Table 1.

Fig. 5. NRe projections to the BLA are recruited and potentiated upon remote fear memory extinction. (a) Schematic representation of the experimental approach and fiber photometry recording implant (top); representative picture of GCaMP6f expression and localization of the optical fiber implant in the NRe (bottom). Scale bar = 100μm. **(b)** (Left) Example traces of photometry signals (reported as dF/F, see Methods) generated by 465 nm (black, Ca^{2+}-dependent) and 405 nm (blue, Ca^{2+}-independent) LED excitation during habituation, recall and the last extinction session. Blue boxes indicate freezing bouts (0.5s ≥ light blue < 1.5s; dark blue ≥1.5s). (Right) Mean dF/F signal ±2s around cessation of freezing (indicated by the dashed line, 0s) for ≥1.5s freezing bouts from the corresponding behavioral session in the left panel. **(c)** (Left) Quantification of dF/F difference before and after freezing end. RM One-way ANOVA, $F(2, 10)=7.99$, $P=0.0084$, multiple comparison, Holm-Sidak, * $P<0.05$, **$p<0.01$, N=6 animals. Two-tailed one-sample t-test (theoretical mean=0), # $P<0.05$, N=6 animals. (Right) Quantification of steepest rise latency relative to freezing end. Two-tailed one-sample t-test (theoretical mean=0), # $P<0.01$, N=6 animals/timepoint. **(d)** (Top) Schematic representation of the NRe→BLA pathway specific optogenetic stimulation strategy and fiber optic implant; (bottom) representative picture of Chronos-GFP expression in NRe neurons projecting to the BLA achieved by co-infection of an *AAV2r-pgk::Cre* bilaterally in the BLA and *AAV1-Syn::FLEX-Chronos-GFP* in the NRe, and localization of the optical fiber implant in the NRe. Scale bar = 100μm. **(e)** (Top) Schematic representation of the behavioral closed-loop optogenetic activation experimental strategy. During experimental extinction, real-time freezing detection triggers NRe photostimulation (20 Hz, 2 s) after each freezing bout of ≥ 1s. (Bottom) Example of freezing cessation upon NRe→BLA photostimulation (blue shading) in an *AAV1-GFP* (Left) and *AAV1-Chronos-GFP* (Right) injected animal. Freezing bouts are ordered by freezing epoch duration. **(f)** Latency to freezing cessation upon NRe→BLA behavioral closed-loop optogenetic stimulation in *AAV1-GFP* and *AAV1-Chronos-GFP* injected animals. Two-tailed t-test (Welch-corrected), $P=0.017$, N=5-7 animals/group. **(g)**

Distribution analysis of latency to freezing cessation from light stimulation onset in animals with *AAV1-GFP* and *AAV1-Chronos-GFP* infection in NRe→BLA neurons (bin width: 300 ms); Kolmogorov-Smirnov test, P = 0.0005, N= 119-151 latencies/behavioral group (5-7 animals/group). **(h)** (Top) Schematic representation of *AAV1-hSyn::Chronos-Tom* injections in the NRe and subsequent *ex vivo* patch-clamp recordings in pyramidal cells from the BLA; (bottom) representative picture of *Chronos-Tom* positive fibers deriving from NRe in the BLA. Scale bar = 250 μm. **(i)** Schematic representation of the experimental setting for *ex vivo* electrophysiology in mice that underwent the spaced extinction paradigm and in control groups. **(j)** (Left) Representative traces of evoked postsynaptic currents (EPSCs) elicited by brief LED pulses in BLA pyramidal cells from mice derived from the four behavioral groups described in **i** (color-coded). Inward currents are AMPA-EPSCs recorded at -70 mV, and outward currents are NMDA-EPSCs recorded at +40 mV. (Right) Values of AMPA/NMDA ratio calculated in BLA pyramidal cells from the four behavioral groups. One-way ANOVA $F(3, 40)=5.234$, $P=0.0038$; multiple comparison, Sidak, * $P<0.05$, ** $P<0.01$, N=8-13 cells recorded from 3-4 mice per behavioral group. **(k**) (Top) experimental timeline for *ex vivo* electrophysiology in mice that underwent the spaced extinction paradigm under chemogenetic inhibition of the NRe. All animals were co-injected with *AAV8-hSyn::hM4Di-mCherry* and *AAV1-hSyn::Chronos-Tom* in the NRe and underwent contextual fear conditioning (CFC) one week later. Thirty days after CFC, the animals underwent memory recall and the spaced extinction procedure under CNO or vehicle treatment (VEH) and *ex vivo* patch-clamp recordings were performed one day later in the absence of CNO/VEH treatment. (Bottom) Representative traces depicting AMPA-EPSCs recorded at -70 mV and NMDA-EPSCs recorded at +40 mV in BLA pyramidal cells from mice derived receiving CNO or VEH treatment during the extinction procedure. (Right) Values of AMPA/NMDA ratio calculated in BLA pyramidal cells from VEH or CNO treated animals. Two-tailed t-test (Welch-corrected), $P=0.0176$, N=9-13 neurons/group (from 3-4 animals per group). **(l)** Experimental timeline (top)

and freezing responses (bottom) during a sub-optimal remote fear memory extinction paradigm. All animals were co-injected with *AAV8-hSyn::hM3Dq-mCherry* and *AAV1-hSyn::Chronos-Tom* in the NRe and underwent contextual fear conditioning (CFC) one week later. Thirty days after CFC, the animals underwent memory recall under CNO or VEH treatment and subsequently received CNO/VEH treatment in their home cage once a day for three days. On the following day a subset of animals was taken for ex-vivo patch clamp recordings while the remaining animals were tested for extinction memory (ET), and two weeks later for spontaneous recovery (SR). Two-way RM ANOVA, VEH vs CNO: $F(1, 13)=11.71$, $P=0.0045$, multiple comparison, Sidak, * $P<0.05$, N=6-9 animals/group. **(m)** (Left) Representative traces depicting AMPA-EPSCs recorded at -70 mV and NMDA-EPSCs recorded at +40 mV in BLA pyramidal cells from mice receiving CNO or VEH treatment during the sub-optimal extinction procedure. (Right) Values of AMPA/NMDA ratio calculated in BLA pyramidal cells from VEH or CNO treated animals. Two-tailed t-test (Welch-corrected), $P=0.0304$, N=14-15 neurons/group (from 3 animals per group). BL, baseline freezing upon novel context exposure; BLA, basolateral amygdala; CFC, contextual fear conditioning; CNO, clozapine-N-oxide; ET, extinction test; Ext, extinction; Hab, habituation; NRe, nucleus reuniens of the thalamus; data are represented as mean ±SEM. Statistical analysis details for each figure panel are reported in Supplementary Table 1.

Fig. 6. NRe inputs to the BLA bidirectionally modulate remote fear memory extinction. **(a)** Schematic representation of the experimental strategy for DREADD-mediated manipulation of NRe-deriving terminals in the BLA. **(b)** Representative picture of hM4Di-mCherry expression in the NRe and cannula placement in the BLA (scale bar = 1mm). **(c)** Selective hM3Dq-mediated activation of NRe deriving fibers in the BLA persistently reduces remote fear memory. CNO/vehicle was locally infused in the amygdala at remote recall and in the home cage once a day for the following 3 days (right). Blue bars indicate CNO exposure. Two-way RM ANOVA, VEH vs CNO: $F(1, 14)=12.67$, $P=0.0031$, multiple comparison, Sidak, ** $P<0.01$, N=8 animals/group. **(d)** Locomotion analysis in an open field arena upon hM3Dq-mediated activation of NRe-deriving terminals in the BLA. Two-tailed t-test, $P=0.518$. N=4 animals/group. **(e)** Selective hM4Di-mediated inhibition of NRe-deriving fibers in the BLA impairs remote fear memory extinction. CNO/vehicle was locally infused in the amygdala at remote recall and extinction. Yellow bars indicate days with CNO or VEH exposure. Two-way RM ANOVA, VEH vs CNO: $F(1, 17)=9.05$, $P=0.0079$, multiple comparison, Sidak, * $P<0.05$, N=8-11 animals/group. **(f)** Locomotion analysis in an open field arena upon hM4Di-mediated inhibition of NRe-deriving terminals in the BLA. Two-tailed t-test, $P=0.762$. N=7-9 animals/group. BLA, basolateral amygdala; BL, baseline freezing upon novel context exposure; CFC, contextual fear conditioning; CNO, clozapine-N-oxide; VEH, vehicle; ET, extinction test; Rec, recall; SR, spontaneous recovery. Data are represented as mean ±SEM. Statistical analysis details for each figure panel are reported in Supplementary Table 1.

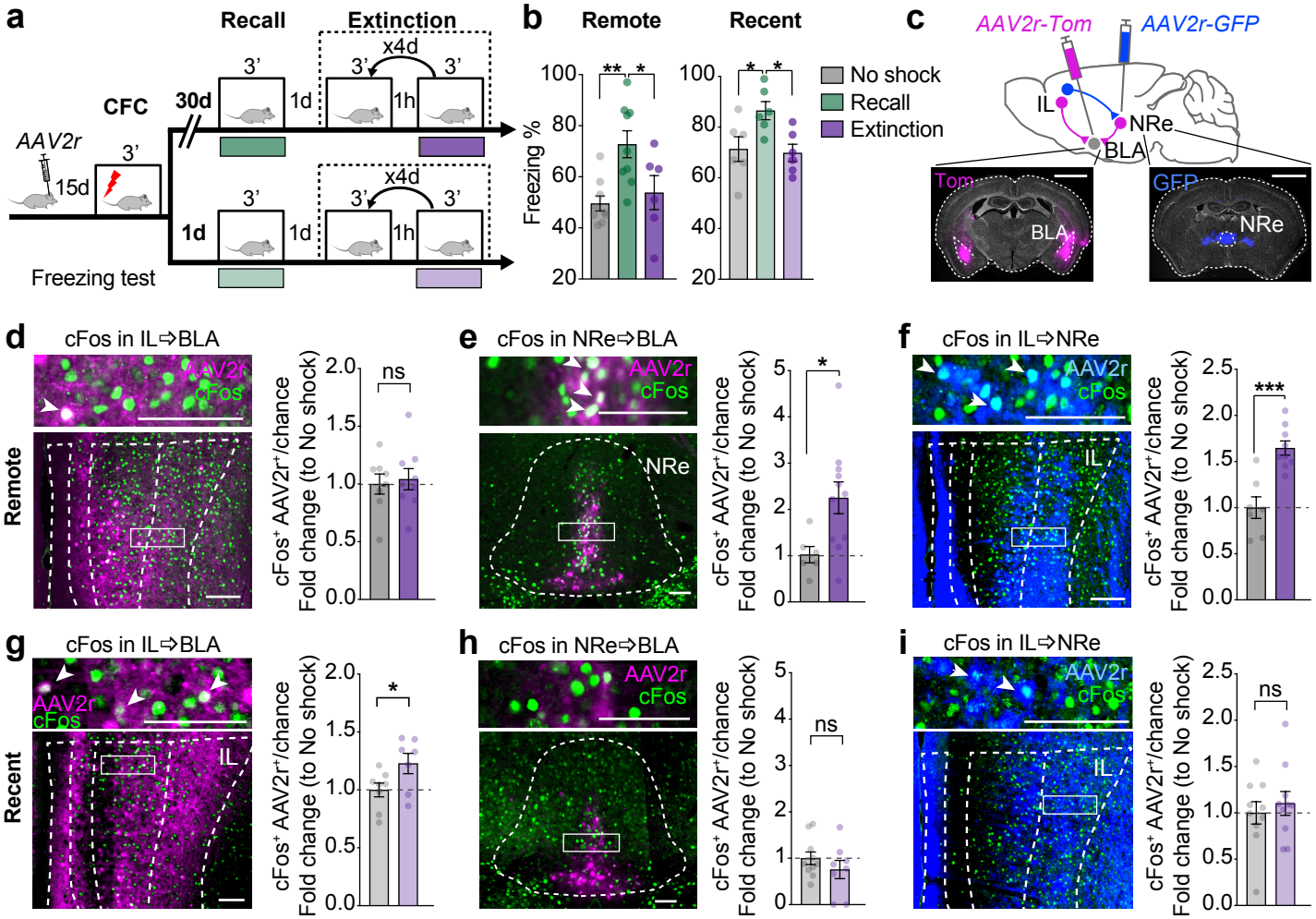
a
Recall
Extinction
CFC
AAV2r
15d
30d
1d
3'
x4d
1h
Freezing test
b
Remote
Recent
Freezing %
No shock
Recall
Extinction
c
AAV2r-Tom
AAV2r-GFP
IL
NRe
BLA
Tom
GFP
d
cFos in IL⇨BLA
Remote
AAV2r
cFos
cFos⁺ AAV2r⁺/chance
Fold change (to No shock)
ns
e
cFos in NRe⇨BLA
NRe
f
cFos in IL⇨NRe
IL
g
cFos in IL⇨BLA
Recent
h
cFos in NRe⇨BLA
i
cFos in IL⇨NRe

Figure 1

Fig. 1. Recent fear memory extinction activates IL to BLA inputs, whereas remote fear extinction recruits an IL→NRe→BLA pathway. (a) Schematic representation of the behavioral paradigm for remote (top) and recent (bottom) fear memory extinction. Fifteen days after viral tracer injection mice underwent contextual fear conditioning (CFC). Thirty days (remote, top) or one day (recent, bottom) later, animals were re-exposed to the conditioned context in the absence of foot shock (Recall) and, subsequently, to the spaced remote fear memory extinction paradigm consisting of two sessions of context exposure per day for four days. Control animals did not receive foot shocks during fear conditioning, but underwent the extinction procedure (No shock). **(b)** Freezing levels during recall and the last extinction session (Extinction) of the remote (left) and recent (right) fear memory extinction paradigm compared to freezing levels in control animals. Remote: One-way ANOVA, $F(2, 21)=7.13$, $P=0.004$, multiple comparison, Holm-Sidak, * $P<0.05$, ** $P<0.01$; Recent: One-way ANOVA, $F(2, 15)=5.32$, $P=0.018$, multiple comparison, Holm-Sidak, * $P<0.05$, ** $P<0.01$. N=6-10 animals/ behavioural group. **(c)** Schematic representation (top) and example pictures (bottom) of the retrograde virus injection strategy. Scale bar: 1mm **(d)** Representative picture (left) and colocalization analysis (right) of retrogradely traced cells from the BLA ($AAV2r^+$) and cells activated in the IL ($cFos^+$) in the remote extinction and the no shock control group. Unpaired t-test, $P=0.748$, N=8-9 animals/behavioral group. **(e)** Example picture (left) and colocalization analysis (right) of retrogradely traced cells from the BLA ($AAV2r^+$) and cells activated in the NRe ($cFos^+$) in the remote extinction and the no shock control group. Unpaired t-test, $P=0.024$, N=6-11 animals/behavioral group. **(f)** Example picture (left) and colocalization analysis (right) of retrogradely traced cells from the NRe ($AAV2r^+$) and cells activated in the IL ($cFos^+$) in the remote extinction and the no shock control group. Unpaired t-test, $P=0.0003$, N=7-9 animals/behavioral group. **(g)** Representative picture (left) and colocalization analysis (right) of retrogradely traced cells from the BLA ($AAV2r^+$) and cells activated in the IL ($cFos^+$) in the recent extinction and the

no shock control group. Unpaired t-test, P=0.0459, N=7-8 animals/behavioral group. **(h)** Example picture (left) and colocalization analysis (right) of retrogradely traced cells from the BLA ($AAV2r^+$) and cells activated in the NRe ($cFos^+$) in the recent extinction and the no shock control group. Unpaired t-test, P=0.31, N=8-10 animals/behavioral group. **(i)** Example picture (left) and colocalization analysis (right) of retrogradely traced cells from the NRe ($AAV2r^+$) and cells activated in the IL ($cFos^+$) in the recent extinction and the no shock control group. Unpaired t-test, P=0.57, N=10 animals/behavioral group; scale bar = 100μm. Arrowheads indicate double positive cells ($AAV2r^+$, $cFos^+$). BLA, basolateral amygdala; CFC, contextual fear conditioning; Ext, extinction; IL, infralimbic cortex; NRe, nucleus reuniens of the thalamus. Data are represented as mean ±SEM. Statistical analysis details for each figure panel are reported in Supplementary Table 1.

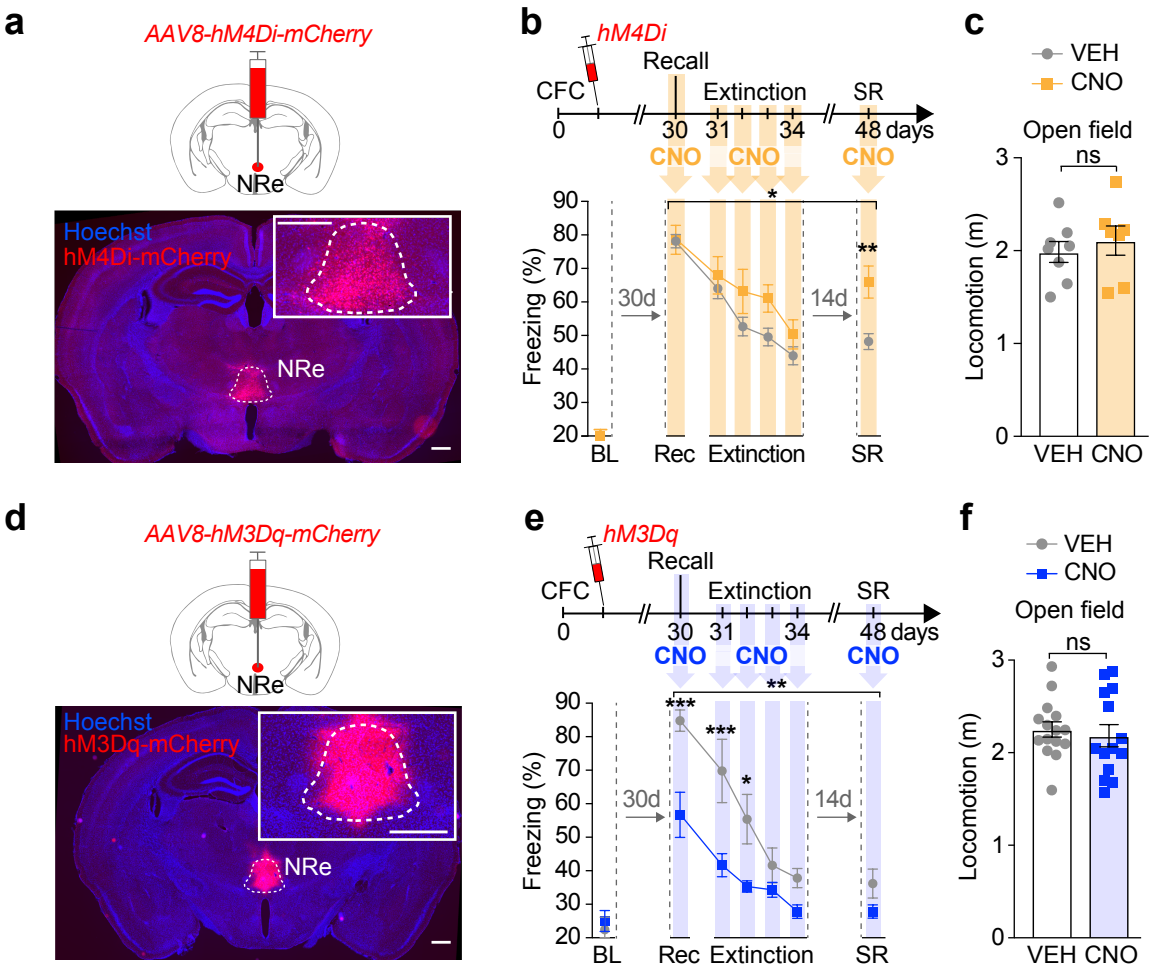
a
AAV8-hM4Di-mCherry
NRe
Hoechst
hM4Di-mCherry
NRe
b
hM4Di
Recall
CFC
Extinction
SR
0
30
31
34
48 days
CNO
CNO
CNO
Freezing (%)
30d
14d
BL
Rec
Extinction
SR
c
VEH
CNO
Open field
ns
Locomotion (m)
VEH
CNO
d
AAV8-hM3Dq-mCherry
NRe
Hoechst
hM3Dq-mCherry
NRe
e
hM3Dq
Recall
CFC
Extinction
SR
0
30
31
34
48 days
CNO
CNO
CNO
Freezing (%)
30d
14d
BL
Rec
Extinction
SR
f
VEH
CNO
Open field
ns
Locomotion (m)
VEH
CNO

Figure 2

Fig. 2. The NRe bidirectionally modulates remote fear memory extinction. (a) (Top) Schematic representation of *AAV8-hM4Di-mCherry* injection in the NRe. (Bottom) Representative picture of hM4Di-mCherry expression in the NRe scale bar = 500μm. **(b)** (Top) Experimental timeline. All animals underwent contextual fear conditioning (CFC) and were injected with *AAV8-hSyn::hM4Di-mCherry* one week later. Thirty days after CFC, the animals underwent memory recall, the spaced extinction procedure and a test for spontaneous recovery of the fear (SR) under CNO or vehicle treatment (VEH). (Bottom) Freezing responses during the remote fear memory extinction paradigm and SR upon hM4Di/CNO-mediated inhibition of the NRe or its vehicle control. Yellow bars indicate days of CNO or VEH administration. Two-way RM ANOVA, VEH vs CNO: $F(1, 45)=5.696$, $P=0.02$, multiple comparison, Sidak, ** $P<0.01$, N=10-37 animals/group. **(c)** Locomotion analysis in an open field arena upon hM4Di/CNO-mediated inhibition of the NRe. Unpaired t-test, $P=0.53$. N=7-8 animals/group. **(d)** (Top) Schematic representation of *AAV8-hM3Dq-mCherry* injection in the NRe. (Bottom) Representative picture of hM3Dq-mCherry expression in the NRe scale bar = 500μm. **(e)** (Top) Experimental timeline. All animals underwent CFC and were injected with *AAV8-CamKII::hM3Dq-mCherry* one week later. Thirty days after CFC, the animals underwent memory recall, the spaced extinction procedure and a SR test under CNO or vehicle treatment. (Bottom) Freezing responses during the remote fear memory extinction paradigm and SR upon hM3Dq-mediated activation of the NRe. Blue bars indicate CNO or VEH exposure. Two-way RM ANOVA, VEH vs CNO: $F(1, 9)=14.01$, $P=0.0046$, multiple comparison, Sidak, * $P<0.05$, ** $P<0.01$, *** $P<0.001$, N=5-6 animals/ behavioral group. **(f)** Locomotion analysis in an open field arena upon hM3Dq-mediated activation of the NRe. Unpaired t-test, $P=0.64$, N=14-15 animals/group. BL, baseline freezing upon novel context exposure; CFC, contextual fear conditioning; CNO, clozapine-N-oxide; NRe, nucleus reuniens of the thalamus; Rec, recall; SR, spontaneous

recovery; VEH, vehicle. Data are represented as mean ±SEM. Statistical analysis details for each figure panel are reported in Supplementary Table 1.

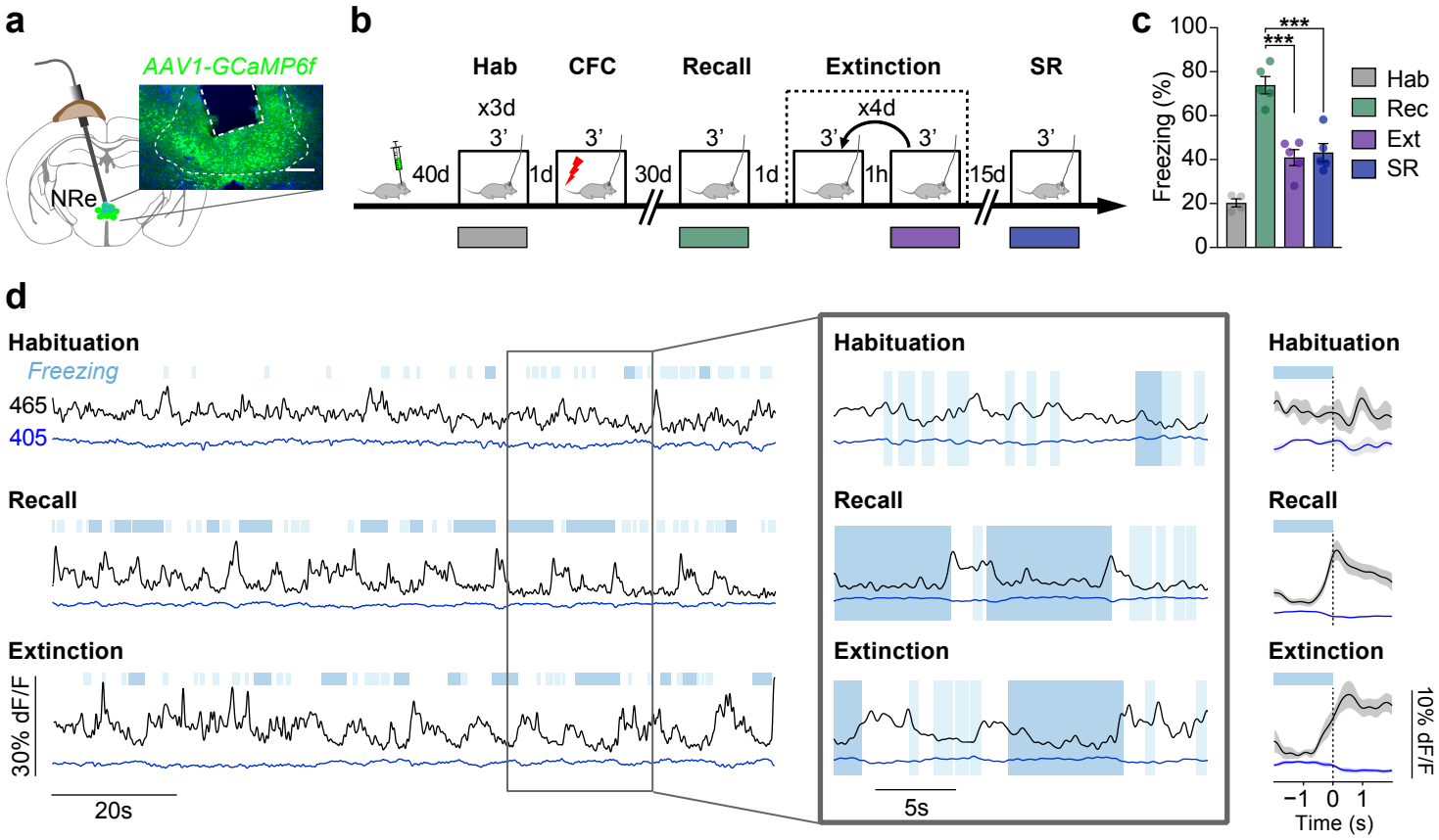
a
AAV1-GCaMP6f
NRe
b
Hab
CFC
Recall
Extinction
SR
x3d
x4d
3'
40d
1d
30d
1h
15d
c
Freezing (%)
Hab
Rec
Ext
SR
***
d
Habituation
Freezing
465
405
Recall
Extinction
30% dF/F
20s
5s
10% dF/F
Time (s)

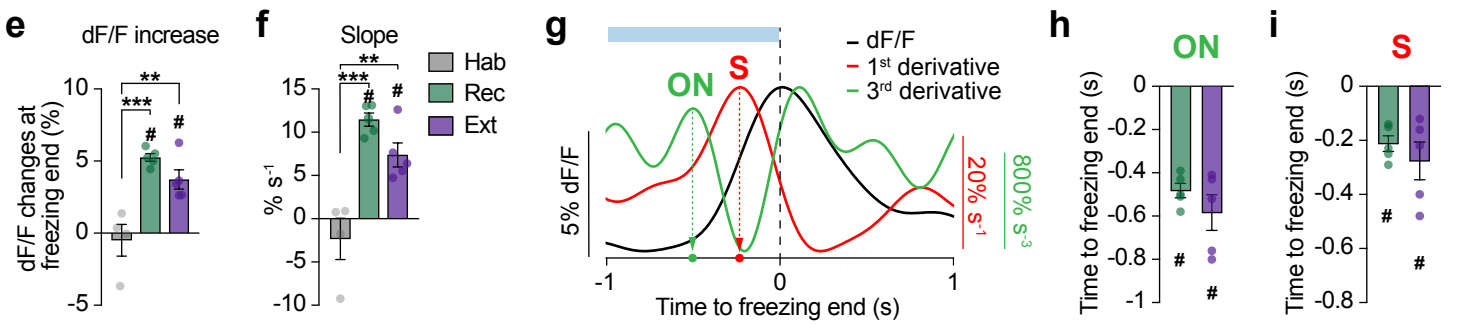
e
dF/F increase
dF/F changes at freezing end (%)
f
Slope
% s-1
Hab
Rec
Ext
g
ON
S
dF/F
1st derivative
3rd derivative
5% dF/F
20% s-1
800% s-3
Time to freezing end (s)
h
ON
Time to freezing end (s)
i
S
Time to freezing end (s)

Figure 3

Fig. 3. Freezing cessation during remote fear memory recall and extinction is accompanied by increased NRe activity. (a) Schematic representation of the fiber photometry recording implant (left) and representative picture of GCaMP6f expression and localization of the optical fiber implant in the NRe (right). Scale bar = 200μm. **(b)** Schematic representation of the experimental setup. Forty days after fiber optic implantation, animals were exposed to the conditioned context in the absence of shock once a day for 3 days and connected to the patch cord for Habituation (Hab). On the following day, mice underwent contextual fear conditioning (CFC). Animals were re-exposed to the conditioned context 30 days later in the absence of foot shock (Recall) and, subsequently, to the spaced extinction paradigm consisting of two sessions of context exposure per day for four days. Fifteen days later animals received an additional context exposure to test for the spontaneous recovery of the fear response (SR). Five minutes before each behavioral session, animals were connected to the patch cord, and photometry recording was started. **(c)** Freezing levels during Habituation, Recall, the last extinction session (Ext) and SR. One-way RM ANOVA for Rec, Ext and SR, $F(2, 8)=31.1$, $P=0.0002$, multiple comparison, Sidak, *** $P<0.001$. N=5 animals. **(d)** (Left) Example traces of photometry signals (reported as dF/F, see Methods) generated by 465 nm (black, Ca^{2+}-dependent) and 405 nm (blue, Ca^{2+}-independent) LED excitation during habituation, recall and the last extinction session. Blue boxes above the traces indicate freezing bouts (0.5s ≥ light blue < 1.5s; dark blue ≥1.5s). (Boxed) Expanded portions of the traces on the left, relating NRe activity and freezing bouts. (Right) Mean dF/F signal ±2s around freezing cessation (indicated by the dashed line, 0s) for ≥1.5s freezing bouts from the corresponding behavioral session in the left panel. **(e)** Quantification of dF/F difference before and after freezing end. One-way ANOVA, $F(2, 11)=16.96$, $P=0.0004$, multiple comparison, Sidak, ** $P<0.01$, *** $P<0.001$, N=4-5 animals/timepoint. Two-tailed one-sample t-test (theoretical mean=0), # $P<0.01$, N=4-5 animals/timepoint. **(f)** Quantification of dF/F mean slope during the 0.4s interval before freezing end. One-way

ANOVA, F(2, 11)=20.25, P=0.0002, multiple comparison, Sidak, ** P<0.01, *** P<0.001, N=4-5 animals/timepoint. Two-tailed one-sample t-test (theoretical mean=0), # P<0.01, N=4-5 animals/timepoint. **(g)** Illustration of the first and third derivative of mean dF/F around freezing end used to calculate the signal onset (ON) and latency of steepest rise (S) relative to freezing cessation (dashed line, 0s). **(h)** Quantification of signal onset latency relative to freezing end. Two-tailed one-sample t-test (theoretical mean=0), # P<0.01, N=5 animals/timepoint. **(i)** Quantification of steepest rise latency relative to freezing end. Two-tailed one-sample t-test (theoretical mean=0), # P<0.05, N=5 animals/timepoint. CFC, contextual fear conditioning; Ext, extinction; Hab, habituation; NRe, nucleus reuniens of the thalamus; Rec, recall; SR, spontaneous recovery. Data are represented as mean ±SEM. Statistical analysis details for each figure panel are reported in Supplementary Table 1.

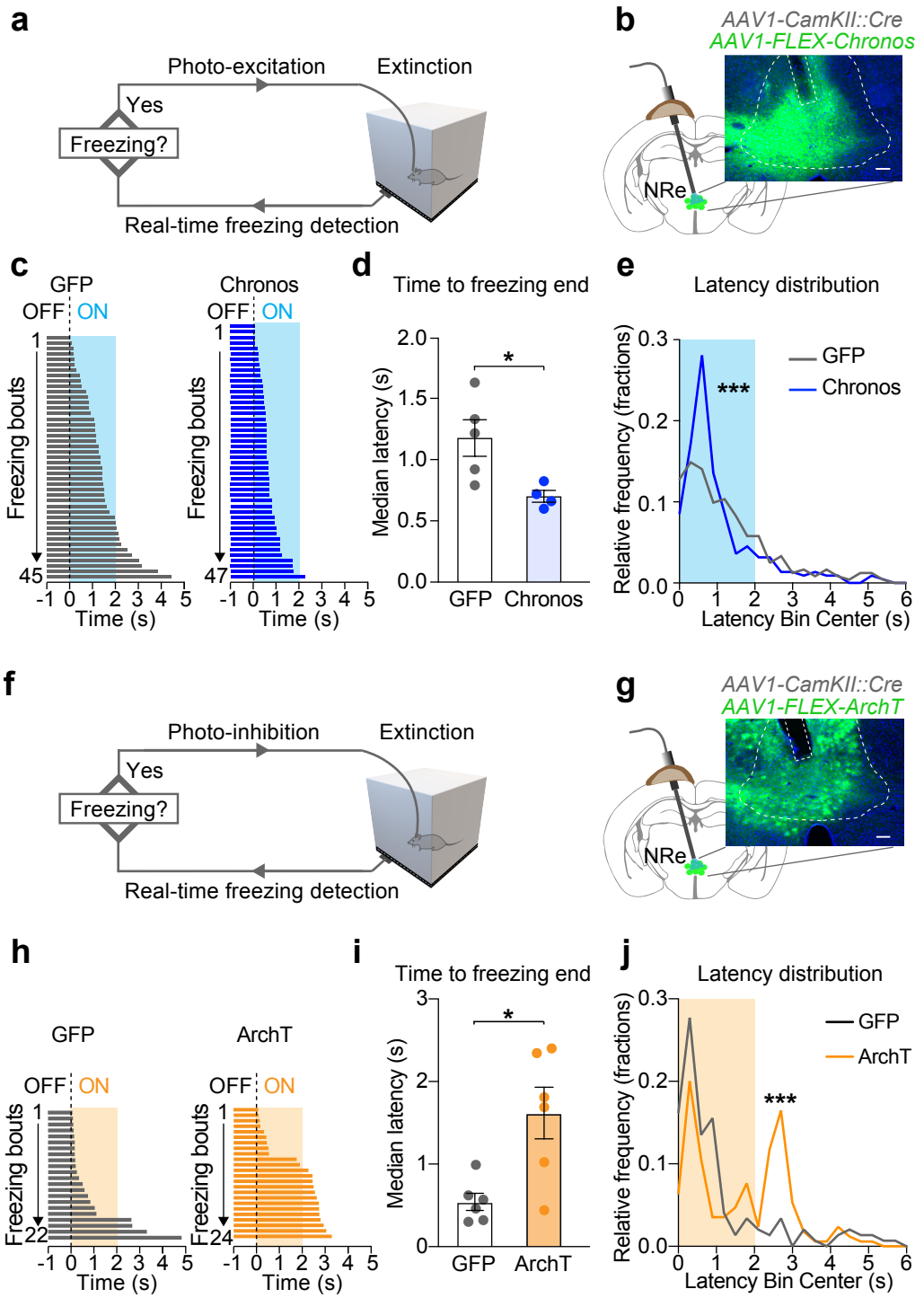
a
Photo-excitation
Extinction
Yes
Freezing?
Real-time freezing detection
b
AAV1-CamKII::Cre
AAV1-FLEX-Chronos
NRe
c
GFP
Chronos
OFF
ON
Freezing bouts
Time (s)
d
Time to freezing end
Median latency (s)
GFP
Chronos
e
Latency distribution
Relative frequency (fractions)
GFP
Chronos
Latency Bin Center (s)
f
Photo-inhibition
Extinction
Yes
Freezing?
Real-time freezing detection
g
AAV1-CamKII::Cre
AAV1-FLEX-ArchT
NRe
h
GFP
ArchT
OFF
ON
Freezing bouts
Time (s)
i
Time to freezing end
Median latency (s)
GFP
ArchT
j
Latency distribution
Relative frequency (fractions)
GFP
ArchT
Latency Bin Center (s)

Figure 4

Fig. 4. Behavioral closed-loop optogenetic manipulation of the NRe during remote fear memory extinction bidirectionally modulates freezing cessation. (a) Schematic representation of the behavioral closed-loop optogenetic activation experimental strategy: Real-time freezing detection triggers NRe photostimulation (20 Hz, 2 s) after each freezing bout of ≥ 1s. **(b)** (Left) Schematic representation of the optogenetic fiber optic implant; (right) representative picture of Chronos-GFP expression in NRe excitatory neurons achieved by co-infection of an *AAV1-CamKII::Cre* and *AAV1-Syn::FLEX-Chronos-GFP*, and localization of the optical fiber implant in the NRe. Scale bar = 100μm. **(c)** Example of freezing cessation upon NRe photostimulation (blue shading) in an *AAV1-GFP* (left) and *AAV1-Chronos-GFP* (right) injected animal. Freezing bouts are ordered by freezing epoch duration. **(d)** Latency to freezing cessation upon NRe behavioral closed-loop optogenetic stimulation in *AAV1-GFP* and *AAV1-Chronos-GFP* injected animals. Two-tailed t-test (Welch-corrected), P=0.03, N=4-5 animals/group. **(e)** Distribution analysis of latency to freezing cessation from light stimulation onset in *AAV1-GFP* and *AAV1-Chronos-GFP* injected animals (bin width: 300 ms); Kolmogorov-Smirnov test, P=0.0007, N=221-242 latencies/behavioral group, 4-5 animals/group. **(f)** Schematic representation of the behavioral closed-loop optogenetic inhibition experimental strategy. Real-time freezing detection triggers NRe photoinhibition (continuous, 2 s) after each freezing bout of ≥ 1s. **(g)** (Left) Schematic representation of the optogenetic fiber optic implant; (right) representative picture of ArchT-GFP expression in NRe excitatory neurons achieved by co-infection of an *AAV1-CamKII::Cre* and *AAV1-Syn::FLEX--ArchT-GFP*, and localization of the optical fiber implant in the NRe. Scale bar = 100μm. **(h)** Example of freezing cessation upon NRe photoinhibition (orange shading) in an *AAV1-GFP* (Left) and *AAV1-ArchT-GFP* (Right) injected animal. Freezing bouts are ordered by freezing epoch duration. **(i)** Latency to freezing cessation upon NRe behavioral closed-loop optogenetic inhibition in *AAV1-GFP* and *AAV1-ArchT-GFP* injected animals. Two-tailed t-test (Welch-corrected), P=0.017, N=6 animals/group. **(j)** Distribution analysis of latency to

freezing cessation from light stimulation onset in *AAV1-GFP* and *AAV1-ArchT-GFP* injected animals (bin width: 300 ms); Kolmogorov-Smirnov test, $P<0.0001$, N=148-170 latencies/behavioral group, 6 animals/group. Data in bar charts are represented as mean ±SEM. Statistical analysis details for each figure panel are reported in Supplementary Table 1.

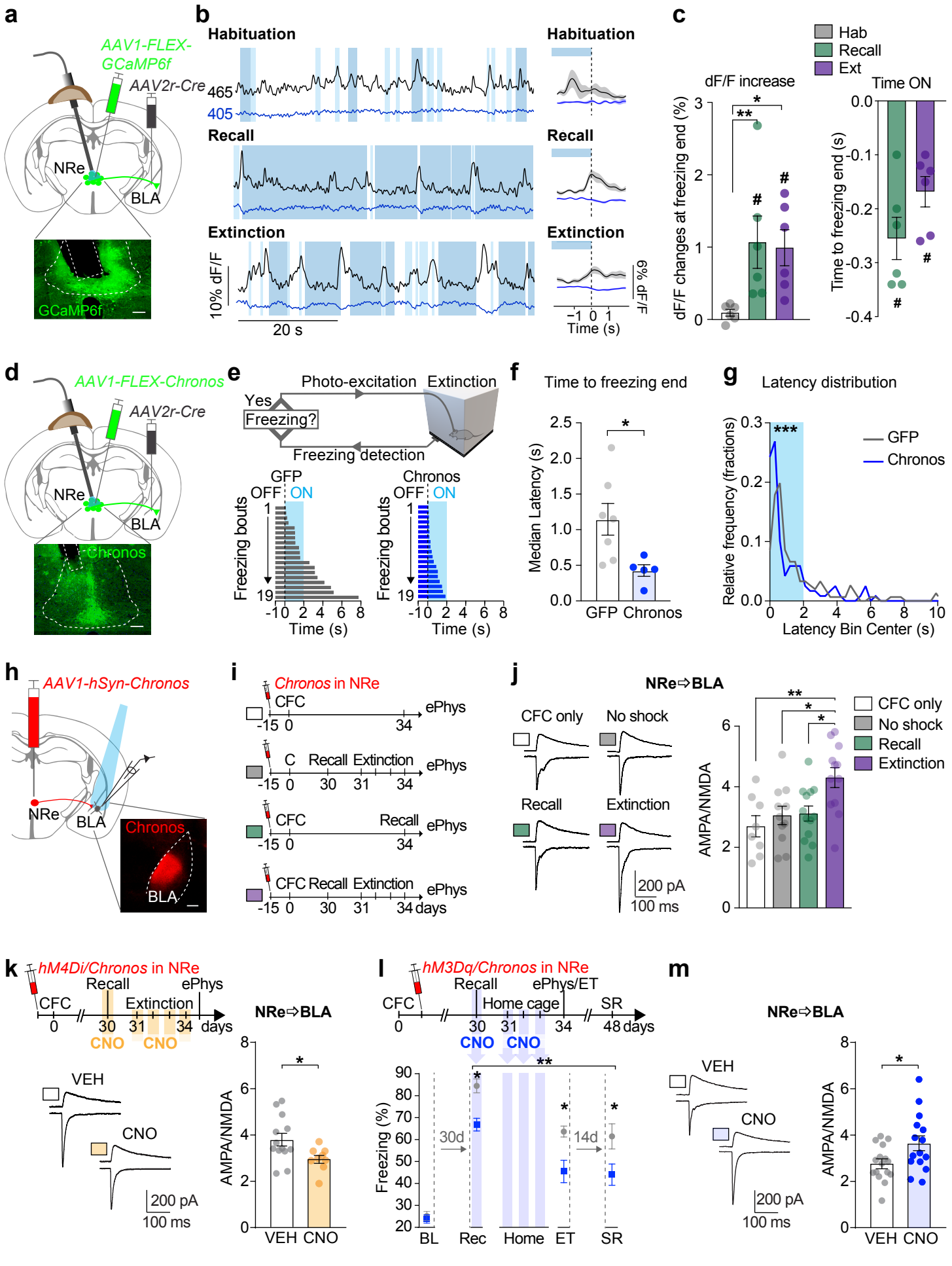
a
AAV1-FLEX-GCaMP6f
AAV2r-Cre
NRe
BLA
GCaMP6f
b
Habituation
Recall
Extinction
465
405
10% dF/F
20 s
6% dF/F
Time (s)
c
Hab
Recall
Ext
dF/F increase
dF/F changes at freezing end (%)
Time ON
Time to freezing end (s)
d
AAV1-FLEX-Chronos
AAV2r-Cre
NRe
BLA
Chronos
e
Photo-excitation
Extinction
Yes
Freezing?
Freezing detection
GFP
Chronos
OFF
ON
Freezing bouts
Time (s)
f
Time to freezing end
Median Latency (s)
GFP
Chronos
g
Latency distribution
Relative frequency (fractions)
GFP
Chronos
Latency Bin Center (s)
h
AAV1-hSyn-Chronos
NRe
BLA
Chronos
BLA
i
Chronos in NRe
CFC
ePhys
C
Recall
Extinction
j
NRe⇨BLA
CFC only
No shock
Recall
Extinction
200 pA
100 ms
AMPA/NMDA
k
hM4Di/Chronos in NRe
Recall
ePhys
CFC
Extinction
CNO
CNO
days
NRe⇨BLA
VEH
CNO
200 pA
100 ms
AMPA/NMDA
VEH
CNO
l
hM3Dq/Chronos in NRe
Recall
ePhys/ET
CFC
Home cage
SR
CNO
CNO
48 days
Freezing (%)
30d
14d
BL
Rec
Home
ET
SR
m
NRe⇨BLA
VEH
CNO
200 pA
100 ms
AMPA/NMDA
VEH
CNO

Figure 5

Fig. 5. NRe projections to the BLA are recruited and potentiated upon remote fear memory extinction. (a) Schematic representation of the experimental approach and fiber photometry recording implant (top); representative picture of GCaMP6f expression and localization of the optical fiber implant in the NRe (bottom). Scale bar = 100μm. **(b)** (Left) Example traces of photometry signals (reported as dF/F, see Methods) generated by 465 nm (black, Ca^{2+}-dependent) and 405 nm (blue, Ca^{2+}-independent) LED excitation during habituation, recall and the last extinction session. Blue boxes indicate freezing bouts (0.5s ≥ light blue < 1.5s; dark blue ≥1.5s). (Right) Mean dF/F signal ±2s around cessation of freezing (indicated by the dashed line, 0s) for ≥1.5s freezing bouts from the corresponding behavioral session in the left panel. **(c)** (Left) Quantification of dF/F difference before and after freezing end. RM One-way ANOVA, $F(2, 10)=7.99$, $P=0.0084$, multiple comparison, Holm-Sidak, * $P<0.05$, **$p<0.01$, N=6 animals. Two-tailed one-sample t-test (theoretical mean=0), # $P<0.05$, N=6 animals. (Right) Quantification of steepest rise latency relative to freezing end. Two-tailed one-sample t-test (theoretical mean=0), # $P<0.01$, N=6 animals/timepoint. **(d)** (Top) Schematic representation of the NRe→BLA pathway specific optogenetic stimulation strategy and fiber optic implant; (bottom) representative picture of Chronos-GFP expression in NRe neurons projecting to the BLA achieved by co-infection of an *AAV2r-pgk::Cre* bilaterally in the BLA and *AAV1-Syn::FLEX-Chronos-GFP* in the NRe, and localization of the optical fiber implant in the NRe. Scale bar = 100μm. **(e)** (Top) Schematic representation of the behavioral closed-loop optogenetic activation experimental strategy. During experimental extinction, real-time freezing detection triggers NRe photostimulation (20 Hz, 2 s) after each freezing bout of ≥ 1s. (Bottom) Example of freezing cessation upon NRe→BLA photostimulation (blue shading) in an *AAV1-GFP* (Left) and *AAV1-Chronos-GFP* (Right) injected animal. Freezing bouts are ordered by freezing epoch duration. **(f)** Latency to freezing cessation upon NRe→BLA behavioral closed-loop optogenetic stimulation in *AAV1-GFP* and *AAV1-Chronos-GFP* injected animals. Two-tailed

t-test (Welch-corrected), P=0.017, N=5-7 animals/group. **(g)** Distribution analysis of latency to freezing cessation from light stimulation onset in animals with *AAV1-GFP* and *AAV1-Chronos-GFP* infection in NRe→BLA neurons (bin width: 300 ms); Kolmogorov-Smirnov test, P = 0.0005, N= 119-151 latencies/behavioral group (5-7 animals/group). **(h)** (Top) Schematic representation of *AAV1-hSyn::Chronos-Tom* injections in the NRe and subsequent *ex vivo* patch-clamp recordings in pyramidal cells from the BLA; (bottom) representative picture of *Chronos-Tom* positive fibers deriving from NRe in the BLA. Scale bar = 250 μm. **(i)** Schematic representation of the experimental setting for *ex vivo* electrophysiology in mice that underwent the spaced extinction paradigm and in control groups. **(j)** (Left) Representative traces of evoked postsynaptic currents (EPSCs) elicited by brief LED pulses in BLA pyramidal cells from mice derived from the four behavioral groups described in **i** (color-coded). Inward currents are AMPA-EPSCs recorded at -70 mV, and outward currents are NMDA-EPSCs recorded at +40 mV. (Right) Values of AMPA/NMDA ratio calculated in BLA pyramidal cells from the four behavioral groups. One-way ANOVA $F(3, 40)=5.234$, $P=0.0038$; multiple comparison, Sidak, * $P<0.05$, ** $P<0.01$, N=8-13 cells recorded from 3-4 mice per behavioral group. **(k**) (Top) experimental timeline for *ex vivo* electrophysiology in mice that underwent the spaced extinction paradigm under chemogenetic inhibition of the NRe. All animals were co-injected with *AAV8-hSyn::hM4Di-mCherry* and *AAV1-hSyn::Chronos-Tom* in the NRe and underwent contextual fear conditioning (CFC) one week later. Thirty days after CFC, the animals underwent memory recall and the spaced extinction procedure under CNO or vehicle treatment (VEH) and *ex vivo* patch-clamp recordings were performed one day later in the absence of CNO/VEH treatment. (Bottom) Representative traces depicting AMPA-EPSCs recorded at -70 mV and NMDA-EPSCs recorded at +40 mV in BLA pyramidal cells from mice derived receiving CNO or VEH treatment during the extinction procedure. (Right) Values of AMPA/NMDA ratio calculated in BLA pyramidal cells from VEH or CNO treated animals. Two-tailed t-test

(Welch-corrected), P=0.0176, N=9-13 neurons/group (from 3-4 animals per group). **(l)** Experimental timeline (top) and freezing responses (bottom) during a sub-optimal remote fear memory extinction paradigm. All animals were co-injected with *AAV8-hSyn::hM3Dq-mCherry* and *AAV1-hSyn::Chronos-Tom* in the NRe and underwent contextual fear conditioning (CFC) one week later. Thirty days after CFC, the animals underwent memory recall under CNO or VEH treatment and subsequently received CNO/VEH treatment in their home cage once a day for three days. On the following day a subset of animals was taken for ex-vivo patch clamp recordings while the remaining animals were tested for extinction memory (ET), and two weeks later for spontaneous recovery (SR). Two-way RM ANOVA, VEH vs CNO: F(1, 13)=11.71, P=0.0045, multiple comparison, Sidak, * P<0.05, N=6-9 animals/group. **(m)** (Left) Representative traces depicting AMPA-EPSCs recorded at -70 mV and NMDA-EPSCs recorded at +40 mV in BLA pyramidal cells from mice receiving CNO or VEH treatment during the sub-optimal extinction procedure. (Right) Values of AMPA/NMDA ratio calculated in BLA pyramidal cells from VEH or CNO treated animals. Two-tailed t-test (Welch-corrected), P=0.0304, N=14-15 neurons/group (from 3 animals per group). BL, baseline freezing upon novel context exposure; BLA, basolateral amygdala; CFC, contextual fear conditioning; CNO, clozapine-N-oxide; ET, extinction test; Ext, extinction; Hab, habituation; NRe, nucleus reuniens of the thalamus; data are represented as mean ±SEM. Statistical analysis details for each figure panel are reported in Supplementary Table 1.

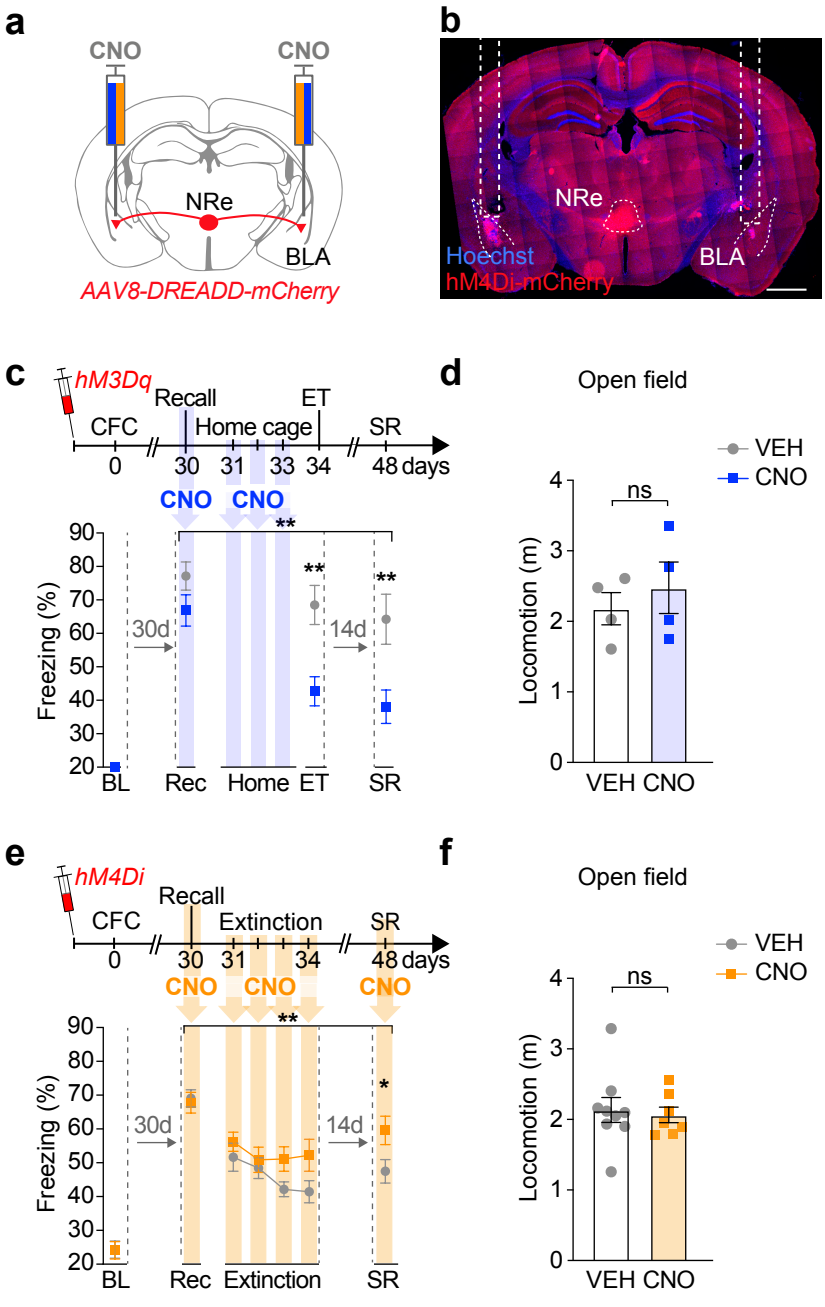
a
CNO
CNO
NRe
BLA
AAV8-DREADD-mCherry
b
NRe
Hoechst
hM4Di-mCherry
BLA
c
hM3Dq
Recall
ET
CFC
Home cage
SR
0
30
31
33
34
48 days
CNO
CNO
**
**
**
Freezing (%)
90
80
70
60
50
40
30
20
30d
14d
BL
Rec
Home
ET
SR
d
Open field
VEH
CNO
ns
Locomotion (m)
4
3
2
1
0
VEH
CNO
e
hM4Di
Recall
CFC
Extinction
SR
0
30
31
34
48 days
CNO
CNO
CNO
**
*
Freezing (%)
90
80
70
60
50
40
30
20
30d
14d
BL
Rec
Extinction
SR
f
Open field
VEH
CNO
ns
Locomotion (m)
4
3
2
1
0
VEH
CNO

Figure 6

Fig. 6. NRe inputs to the BLA bidirectionally modulate remote fear memory extinction. **(a)** Schematic representation of the experimental strategy for DREADD-mediated manipulation of NRe-deriving terminals in the BLA. **(b)** Representative picture of hM4Di-mCherry expression in the NRe and cannula placement in the BLA (scale bar = 1mm). **(c)** Selective hM3Dq-mediated activation of NRe deriving fibers in the BLA persistently reduces remote fear memory. CNO/vehicle was locally infused in the amygdala at remote recall and in the home cage once a day for the following 3 days (right). Blue bars indicate CNO exposure. Two-way RM ANOVA, VEH vs CNO: $F(1, 14)=12.67$, $P=0.0031$, multiple comparison, Sidak, ** $P<0.01$, N=8 animals/group. **(d)** Locomotion analysis in an open field arena upon hM3Dq-mediated activation of NRe-deriving terminals in the BLA. Two-tailed t-test, $P=0.518$. N=4 animals/group. **(e)** Selective hM4Di-mediated inhibition of NRe-deriving fibers in the BLA impairs remote fear memory extinction. CNO/vehicle was locally infused in the amygdala at remote recall and extinction. Yellow bars indicate days with CNO or VEH exposure. Two-way RM ANOVA, VEH vs CNO: $F(1, 17)=9.05$, $P=0.0079$, multiple comparison, Sidak, * $P<0.05$, N=8-11 animals/group. **(f)** Locomotion analysis in an open field arena upon hM4Di-mediated inhibition of NRe-deriving terminals in the BLA. Two-tailed t-test, $P=0.762$. N=7-9 animals/group. BLA, basolateral amygdala; BL, baseline freezing upon novel context exposure; CFC, contextual fear conditioning; CNO, clozapine-N-oxide; VEH, vehicle; ET, extinction test; Rec, recall; SR, spontaneous recovery. Data are represented as mean ±SEM. Statistical analysis details for each figure panel are reported in Supplementary Table 1.